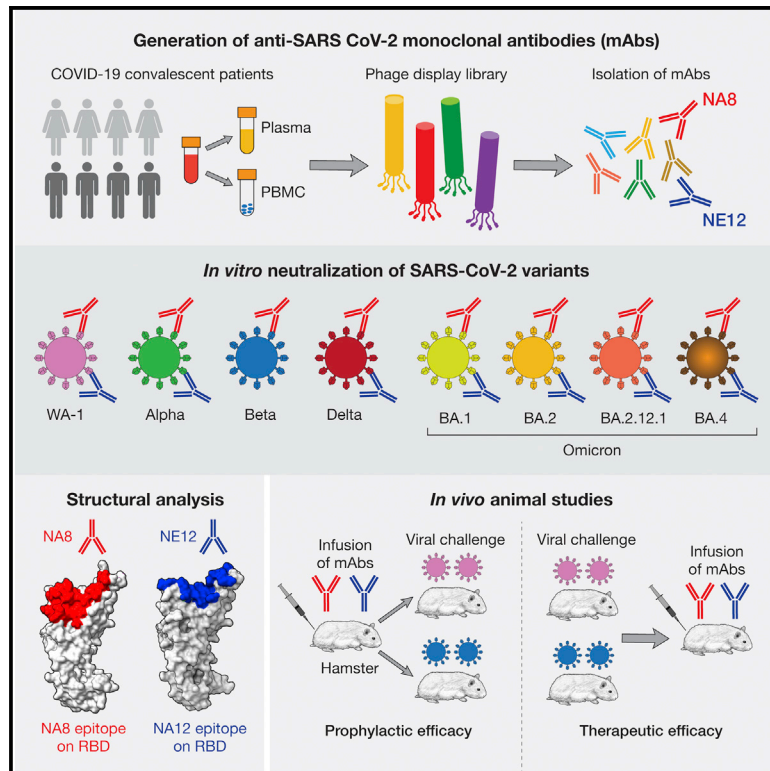


## Potent monoclonal antibodies neutralize Omicron sublineages and other SARS-CoV-2 variants

### Graphical abstract



### Authors

Zhaochun Chen, Peng Zhang, Yumiko Matsuoka, ..., Ursula J. Buchholz, Paolo Lusso, Patrizia Farci

### Correspondence

zchen@niaid.nih.gov (Z.C.), pfarci@niaid.nih.gov (P.F.)

### In brief

The emergence of new SARS-CoV-2 variants that escape neutralization can jeopardize the efficacy of vaccines and therapeutic antibodies. Chen et al. report the isolation of potent human antibodies that neutralize emerging variants of concern, including various Omicron sublineages. These antibodies show prophylactic and therapeutic efficacy in the hamster model.

### Highlights

- Monoclonal antibodies are isolated from COVID-19 convalescent patients
- NA8 and NE12 potently neutralize newly emerging SARS-CoV-2 variants of concern
- Structural analysis reveals a unique conserved binding epitope for NA8
- NA8 and NE12 show prophylactic and therapeutic efficacy in the Syrian hamster model



## Article

# Potent monoclonal antibodies neutralize Omicron sublineages and other SARS-CoV-2 variants

Zhaochun Chen,<sup>1,\*</sup> Peng Zhang,<sup>2</sup> Yumiko Matsuoka,<sup>3,10</sup> Yaroslav Tsybovsky,<sup>4,10</sup> Kamille West,<sup>5</sup> Celia Santos,<sup>3</sup> Lisa F. Boyd,<sup>6</sup> Hanh Nguyen,<sup>1</sup> Anna Pomerrenke,<sup>1</sup> Tyler Stephens,<sup>4</sup> Adam S. Olia,<sup>7</sup> Baoshan Zhang,<sup>7</sup> Valeria De Giorgi,<sup>5</sup> Michael R. Holbrook,<sup>8</sup> Robin Gross,<sup>8</sup> Elena Postnikova,<sup>8</sup> Nicole L. Garza,<sup>9</sup> Reed F. Johnson,<sup>9</sup> David H. Margulies,<sup>6</sup> Peter D. Kwong,<sup>7</sup> Harvey J. Alter,<sup>5</sup> Ursula J. Buchholz,<sup>3</sup> Paolo Lusso,<sup>2</sup> and Patrizia Farci<sup>1,11,\*</sup>

<sup>1</sup>Hepatic Pathogenesis Section, Laboratory of Infectious Diseases, National Institute of Allergy and Infectious Diseases, National Institutes of Health, Bethesda, MD, USA

<sup>2</sup>Laboratory of Immunoregulation, National Institute of Allergy and Infectious Diseases, National Institutes of Health, Bethesda, MD, USA

<sup>3</sup>RNA Viruses Section, Laboratory of Infectious Diseases, National Institute of Allergy and Infectious Diseases, National Institutes of Health, Bethesda, MD, USA

<sup>4</sup>Cancer Research Technology Program, Leidos Biomedical Research, Inc., Frederick National Laboratory for Cancer Research, Frederick, MD, USA

<sup>5</sup>Department of Transfusion Medicine, NIH Clinical Center, National Institutes of Health, Bethesda, MD, USA

<sup>6</sup>Molecular Biology Section, Laboratory of Immune System Biology, National Institute of Allergy and Infectious Diseases, National Institutes of Health, Bethesda, MD, USA

<sup>7</sup>Vaccine Research Center, National Institute of Allergy and Infectious Diseases, National Institutes of Health, Bethesda, MD, USA

<sup>8</sup>National Institute of Allergy and Infectious Diseases (NIAID) Integrated Research Facility, National Institutes of Health, Frederick, MD, USA

<sup>9</sup>SARS-CoV-2 Virology Core, Laboratory of Viral Diseases, National Institute of Allergy and Infectious Diseases, National Institutes of Health, Bethesda, MD, USA

<sup>10</sup>These authors contributed equally

<sup>11</sup>Lead contact

\*Correspondence: [zchen@niaid.nih.gov](mailto:zchen@niaid.nih.gov) (Z.C.), [pfarci@niaid.nih.gov](mailto:pfarci@niaid.nih.gov) (P.F.)

<https://doi.org/10.1016/j.celrep.2022.111528>

## SUMMARY

The emergence and global spread of the SARS-CoV-2 Omicron variants, which carry an unprecedented number of mutations, raise serious concerns due to the reduced efficacy of current vaccines and resistance to therapeutic antibodies. Here, we report the generation and characterization of two potent human monoclonal antibodies, NA8 and NE12, against the receptor-binding domain of the SARS-CoV-2 spike protein. NA8 interacts with a highly conserved region and has a breadth of neutralization with picomolar potency against the Beta variant and the Omicron BA.1 and BA.2 sublineages and nanomolar potency against BA.2.12.1 and BA.4. Combination of NA8 and NE12 retains potent neutralizing activity against the major SARS-CoV-2 variants of concern. Cryo-EM analysis provides the structural basis for the broad and complementary neutralizing activity of these two antibodies. We confirm the *in vivo* protective and therapeutic efficacies of NA8 and NE12 in the hamster model. These results show that broad and potent human antibodies can overcome the continuous immune escape of evolving SARS-CoV-2 variants.

## INTRODUCTION

The ongoing coronavirus disease 2019 (COVID-19) pandemic, caused by severe acute respiratory syndrome coronavirus 2 (SARS-CoV-2), has triggered a devastating global health, social, and economic crisis, with more than 1 million deaths in the United States and over 6.5 million worldwide (<https://coronavirus.jhu.edu>; The Johns Hopkins Coronavirus Resource Center Home Page, 2022). Effective vaccines against SARS-CoV-2 have been developed and deployed at an unprecedented pace, but hesitancy in vaccination and a limited supply in developing countries have made the fight against SARS-CoV-2 particularly challenging. The RNA nature and broad circulation of this virus enable the accumulation of mutations (Telenti et al., 2021;

Yewdell, 2021), leading to the continuous emergence of variants with increased transmissibility or pathogenicity as well as resistance to monoclonal antibodies (mAbs) and vaccine-elicited antibodies (Corti et al., 2021; Davies et al., 2021; Wang et al., 2021; Wibmer et al., 2021), highlighting the need for effective therapeutic and preventive measures with a broad spectrum of action.

As a result of viral evolution, the initial SARS-CoV-2 lineages identified early during the pandemic in Wuhan, China (Zhou et al., 2020), have progressively been replaced by several variants of concern, such as B.1.1.7 (Alpha), B.1.351 (Beta), P.1 (Gamma), B.1.617.2 (Delta) and, most recently, B.1.1.529 (Omicron). In particular, the latter is raising major concern worldwide because it has an unprecedented number of mutations, and it has rapidly spread across the globe (Bowen et al., 2022a;



Bruel et al., 2022; Greaney et al., 2021; Iketani et al., 2022; Lusvardi et al., 2021; Piccoli et al., 2020; Takashita et al., 2022; Yamasoba et al., 2022; Yu et al., 2022; Zhou et al., 2022). It comprises several distinct sublineages (World Health Organization, <https://www.who.int/publications/m/item/weekly-epidemiological-update-on-covid-19-1-february-2022>). The original Omicron variant, BA.1, was first documented in South Africa in November 2021 and became in a short time the predominant variant worldwide (World Health Organization, Classification of Omicron [B.1.1.529]: SARS-CoV-2 Variant of Concern [2021]). This variant has more than 30 mutations in the spike (S) protein (Elbe and Buckland-Merrett, 2017), 15 of which are located within the receptor-binding domain (RBD), the main target of neutralizing antibodies (Greaney et al., 2021; Piccoli et al., 2020). Most of these mutations are unique to this variant. Consistent with this high degree of genetic heterogeneity, the Omicron sublineage BA.1 has reduced or abrogated sensitivity to neutralization by most mAbs, convalescent sera, and vaccine-elicited antibodies (Aggarwal et al., 2021; Cameroni et al., 2022; Cao et al., 2022a; Cele et al., 2022; Dejnirattisai et al., 2021; Doria-Rose et al., 2021; Lusvardi et al., 2021; Mannar et al., 2022; Planas et al., 2022; Wilhelm et al., 2021). As of March 2022, however, the BA.2 sublineage is rapidly replacing BA.1 to become the dominant variant in several areas of the world, including most European countries, India, Pakistan, the Philippines, New Zealand, and South Africa (CoVariants, Overview of Variants/Mutations, March 25, 2022; <https://covariants.org>). BA.2 shares 21 mutations with BA.1, but these two sublineages contain 8 and 13 unique mutations, respectively, in the spike protein. BA.2 has a significantly reduced sensitivity to neutralization by sera from convalescent patients or vaccinated individuals to a degree comparable to that reported for BA.1 (Bowen et al., 2022b; Iketani et al., 2022; Yamasoba et al., 2022; Yu et al., 2022). In addition, BA.2 has shown marked resistance to several mAbs tested, including sotrovimab, which was shown to retain activity against BA.1 (Bruel et al., 2022; Iketani et al., 2022; Takashita et al., 2022; Zhou et al., 2022). Thus, albeit related, these two sublineages exhibit different sensitivity to mAbs and vaccine-elicited antibodies. More recently, three additional Omicron sublineages have emerged, BA.2.12.1, BA.4, and BA.5, and they have rapidly replaced BA.1 and BA.2 worldwide, accounting for the vast majority of new infections globally (World Health Organization, <https://www.who.int/publications/m/item/weekly-epidemiological-update-on-covid-19-20-july-2022>). The BA.4 and BA.5 lineages have an identical spike protein and differ only outside the spike region (Tegally, 2022). As seen with the initial Omicron variants, these newly emerged sublineages show even stronger escape from neutralizing antibodies elicited by both vaccination and natural infection (Bowen et al., 2022b; Cao et al., 2022b; Hachmann et al., 2022; Qu et al., 2022; Shrestha et al., 2022). The reduced effectiveness of current therapeutic antibodies and vaccines against Omicron subvariants, the rapid spread of these variants worldwide, and the limited rate of vaccination in developing countries highlight the urgent global need for the discovery of broadly neutralizing antibodies against SARS-CoV-2.

In this study, we took advantage of our extensive experience in generating mAbs using combinatorial phage-display library technology (Chen et al., 2006, 2018) to derive mAbs from conva-

lescent COVID-19 donors with high neutralization titers. We report the isolation of ultrapotent mAbs that neutralize diverse and highly transmissible SARS-CoV-2 variants of concern, including the difficult-to-neutralize Beta and Omicron sublineages. To further validate our data, we compared side by side the neutralizing activity of our most potent mAbs with that of seven clinically approved mAbs, which confirmed the breadth and potency of our mAbs. Cryo-electron microscopy provided the structural basis for their broad reactivity and potency. Finally, we demonstrated the protective and therapeutic activity of our mAbs in a hamster preclinical model. Overall, this study uncovers potent mAbs, which may be utilized against both present and future SARS-CoV-2 variants of concern that will continue to emerge.

## RESULTS

### Generation and characterization of anti-SARS-CoV-2 monoclonal antibodies using phage-display libraries from COVID-19 convalescent patients

To generate mAbs against the SARS-CoV-2 spike protein by using combinatorial phage-display libraries, peripheral blood samples were collected from 12 convalescent COVID-19 plasma donors with high neutralizing serum antibody titers against SARS-CoV-2 (De Giorgi et al., 2021) (Table S1). Total RNA was extracted from peripheral blood mononuclear cells (PBMC) and used for the construction of phage-display Fab libraries (Figure 1A). A total of four phage-display Fab libraries, derived from either a single donor or multiple donors combined, were constructed, each consisting of  $10^7$  to  $10^9$  individual clones (Figure S1). Three sequential cycles of panning were carried out to enrich for specific clones using a stabilized trimeric spike protein (S-2P) derived from the original SARS-CoV-2 strain, Wuhan-Hu-1 (GenBank: MN908947; S protein sequence identical to that of the of USA/WA-1/2020 [WA-1]; GenBank: MN985325) (Wrapp et al., 2020). Subsequent screening of 672 individual clones by ELISA resulted in the identification of 538 clones that specifically bound to the S-2P protein. DNA sequencing identified 18 unique clones with distinct sequences. These clones were subcloned and expressed both as soluble Fabs and as complete IgG1 antibodies. The binding specificity of the cloned IgGs was confirmed by ELISA (Figure 1B). The binding affinity of the 18 Fabs for the soluble S-2P trimer was further assessed by surface plasmon resonance (SPR). Six Fabs showed either poor or no binding by SPR, while the remaining 12 exhibited high-affinity binding with equilibrium dissociation constants ( $K_D$ ) in the picomolar range for 10 and in the low nanomolar range for 2 (Figure S2; Table S2).

Genetic analysis of V genes of all 18 mAbs indicated that the clones primarily used the variable heavy chain (VH) genes VH1-2 and VH1-69 and the variable light chain (VK) gene VK1-39 (Figures 1C and 1D; Table S3). The dominant use of these VH genes for SARS-CoV-2 S-specific antibodies is consistent with previous studies (Andreano et al., 2021; Yuan et al., 2021). In comparison, the frequency of VH1-2 and VK1-39 gene usage only ranks 23 and 6, respectively, in the B cell repertoire of healthy individuals (Boyd et al., 2010; Prabhakaran et al., 2012), suggesting that certain germline genes are

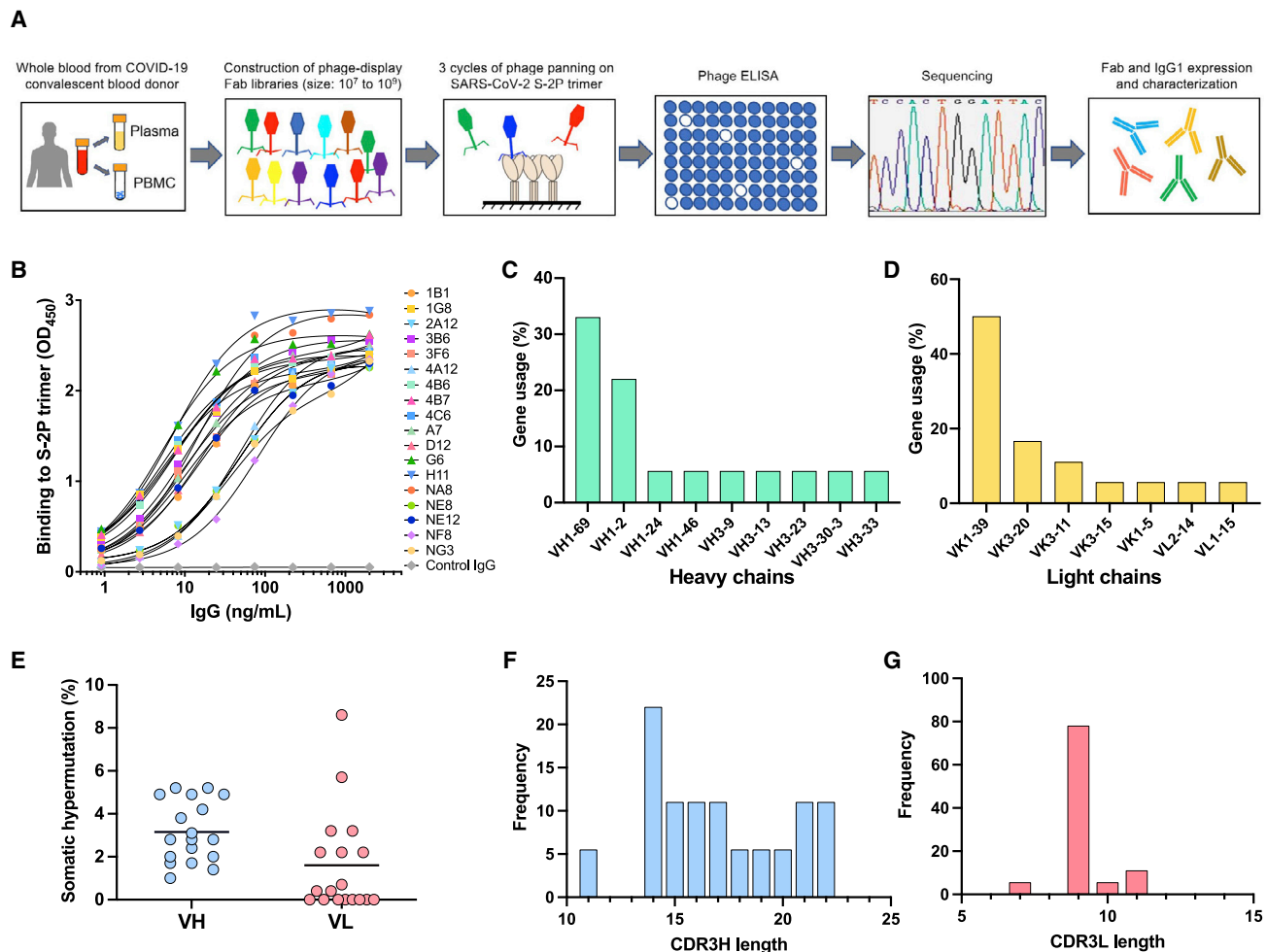


**Figure 1. Study design and characterization of monoclonal antibodies against the SARS-CoV-2 spike protein**

(A) Schematic design of the different phases of combinatorial phage-display library production and screening leading to the development of SARS-CoV-2 neutralizing antibodies (mAbs).

(B) Normalized binding of 18 mAbs to a stabilized SARS-CoV-2 spike protein trimer, S-2P, in ELISA; OD denotes optical density.

(C and D) V-gene usage of (C) heavy chains and (D) light chains of 18 mAbs against the SARS-CoV-2 spike protein.

(E) Rate of somatic hypermutation of V genes of heavy chains (VH) and light chains (VL) of 18 mAbs.

(F and G) Amino acid length of the CDR3 loop of the (F) heavy (CDR3H) and (G) light chain (CDR3L) of 18 mAbs.

naturally favored for binding to the S protein of SARS-CoV-2. Notably, the selected antibodies had very limited somatic hypermutation (SHM) with a median frequency of 3.2% in VH and 1.6% in VL (Figure 1E). These findings are consistent with previous studies, which reported the isolation of anti-SARS-CoV-2 antibodies in nearly germline configuration (Kreye et al., 2020; Liu et al., 2020; Zost et al., 2020b). The length distribution of the complementarity-determining region 3 (CDR3) in both the heavy and light chains was in line with previous observations (Figures 1F and 1G), although we found an unusual bimodal distribution of CDR3 length as opposed to the typical bell-shaped distribution in CDRL3 (Figures 1F and 1G). No correlation was found between SHM frequency in VH and binding affinity, further supporting the notion that certain germline antibody genes are naturally fit for targeting the S protein.

### Potent neutralization of diverse SARS-CoV-2 variants of concern

The neutralizing activity of 18 mAbs was evaluated using a pseudotype virus neutralization assay (Corbett et al., 2020a). Eleven mAbs showed potent neutralizing activity against the original SARS-CoV-2 strain (WA-1), seven with half-maximal inhibitory concentration ( $IC_{50}$ ) values in the picomolar range, below 10 ng/mL (Figure 2A), which is comparable to the potency of the best-in-class mAbs (Baum et al., 2020b; Hansen et al., 2020; Jones et al., 2021). Competition ELISA showed that all the 11 neutralizing mAbs were specific for the RBD domain (Figure S3). Cross-competition ELISA using Fab fragments and complete IgG showed high levels of cross-competition among the 11 neutralizing mAbs with the exception of two, 1G8 and 3F6, which cross-competed only between each other (Figure S4). Next, we tested the neutralizing activity of the 18 mAbs against

A

mAb	Neutralization (IC <sub>50</sub> , µg/mL)							
	WA-1	Alpha	Beta	Delta	Omicron BA.1	Omicron BA.2	Omicron BA.4	Omicron BA.2.12.1
G6	>10	>10	>10	>10	>10	1,453	2,000	0.222
4A12	>10	>10	>10	>10	>10	>10	>10	>10
4B7	>10	>10	>10	>10	>10	>10	>10	>10
A7	>10	>10	>10	>10	>10	>10	>10	>10
1B1	>10	>10	>10	>10	>10	>10	>10	>10
4C6	>10	>10	>10	>10	>10	>10	>10	>10
H11	>10	>10	>10	>10	10,000	10,000	>10	12,000
1G8	0.034	0.100	0.097	0.006	>10	>10	>10	>10
2A12	0.004	0.003	>10	0.008	2,561	7,672	>10	>10
3F6	0.019	0.052	0.079	0.001	1,892	8,063	6,500	7,400
3B6	0.008	0.012	10,000	0.034	0.058	0.042	>10	0.816
4B6	0.027	0.039	0.146	>10	0.530	0.366	>10	>10
D12	0.007	0.013	>10	>10	6,500	>10	>10	12,000
NA8	0.008	0.002	0.004	0.450	0.005	0.008	5,701	0.512
NE8	0.009	0.009	>10	0.002	>10	>10	>10	>10
NE12	0.003	0.004	>10	0.001	2,819	0.498	0.412	1,742
NF8	0.031	0.038	>10	3,000	>10	>10	>10	>10
NG3	0.007	0.008	>10	0.005	>10	>10	>10	>10

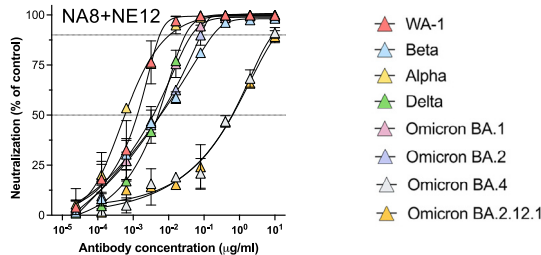
B

mAb	Neutralization (IC <sub>50</sub> , µg/mL)							
	WA-1	Alpha	Beta	Delta	Omicron BA.1	Omicron BA.2	Omicron BA.4	Omicron BA.2.12.1
REGN10933	0.002	0.003	>10	0.001	>10	>10	>10	>10
REGN10987	0.009	0.001	0.002	0.003	>10	0.669	0.358	0.544
LY-CoV555	0.003	0.004	>10	3,000	>10	>10	>10	>10
LY-CoV016	0.019	0.371	>10	0.005	>10	>10	>10	>10
COV2-2196	0.001	0.001	0.004	0.001	0.139	0.309	>10	0.055
COV2-2130	0.001	0.001	0.004	0.015	0.663	0.005	0.040	0.008
S309	0.184	0.254	0.065	0.244	0.371	1,454	1,732	1,774

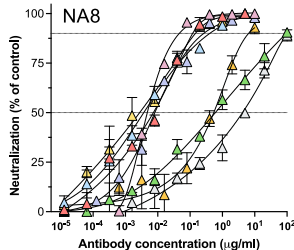
C

mAb combination	Neutralization (IC <sub>50</sub> , µg/mL)					IC <sub>50</sub> (µg/ml)
	WA-1	Omicron BA.1	Omicron BA.2	Omicron BA.4	Omicron BA.2.12.1	
NA8+NE12	0.0008	0.0036	0.0042	0.451	0.511	>10
REGN10933 + REGN10987	0.0009	>10	0.2320	0.334	0.225	10-1
LY-CoV555 + LY-CoV016	0.0015	>10	>10	>10	>10	1-0.1
COV2-2196 + COV2-2130	0.0007	0.0440	0.0060	0.035	0.005	0.1-0.01

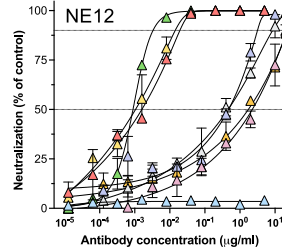
H



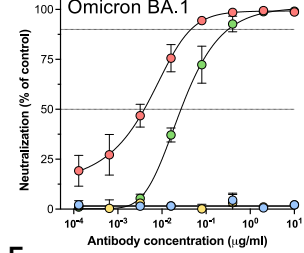
I



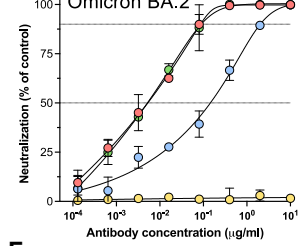
J



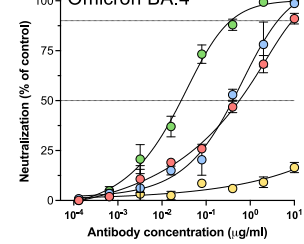
D



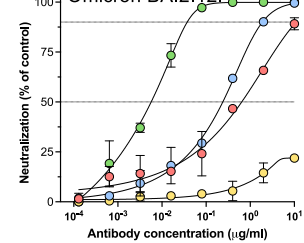
E



F



G



(legend on next page)

the original North American founder strain, WA-1, as well as major variants of concern of global relevance, namely, B.1.1.7/Alpha, B.1.351/Beta, B.1.617.2/Delta, and Omicron BA.1, BA.2, BA.4, and BA.2.12.1 sublineages. All the 11 mAbs that potently neutralized the WA-1 strain retained potent activity against the Alpha variant; seven of them also neutralized the Delta variant in the picomolar range (Figure 2A). In contrast, most of the mAbs were ineffective against the Beta variant with only four retaining high neutralizing activity. Of note, one of them, NA8, neutralized Beta at picomolar concentration. Notably, NA8 also potently neutralized both Omicron BA.1 and BA.2 sublineages, which contain an unprecedented number of mutations within the S protein and are completely or partially resistant to most neutralizing mAbs as well as to serum from convalescent or vaccinated subjects (Aggarwal et al., 2021; Cameroni et al., 2022; Cao et al., 2022b; Cele et al., 2022; Dejnirattisai et al., 2022; Doria-Rose et al., 2021; Mannar et al., 2022; Planas et al., 2022; Wilhelm et al., 2021), with IC<sub>50</sub> values in the picomolar range (Figure 2A). In addition, NA8 also neutralized at nanomolar concentrations the recently emerged BA.2.12.1 and BA.4 sublineages. Six additional mAbs neutralized different Omicron sublineages, although only one (3B6) was active in the picomolar range against BA.1 and BA.2 (Figure 2A).

Next, we compared our antibodies with a panel of mAbs approved for clinical use. Among seven clinical mAbs evaluated, we found that four, namely, REGN-10933 (casirivimab), REGN-10987 (imdevimab) (Baum et al., 2020b; Hansen et al., 2020), LY-CoV555 (bamlanivimab) (Jones et al., 2021), and LY-CoV016 (etesevimab) (Shi et al., 2020), had no detectable neutralizing activity against Omicron BA.1, while three, namely, S309 (sotrovimab) (Cameroni et al., 2022; Cao et al., 2022a; Cathcart et al., 2021), AZD8895/COV2-2196 (tixagevimab), and AZD1061/COV2-2130 (cilgavimab) (Zost et al., 2020a), showed neutralizing activity but were remarkably less potent than NA8 (93-, 166-, and 35-fold, respectively) (Figure 2B). Against the BA.2, BA.2.12.1, and BA.4 Omicron sublineages, only one of the approved antibodies, COV2-2130, retained potent neutralizing activity (Figure 2B).

Clinically approved mAbs are generally used in combination to ensure coverage against multiple variants (Du et al., 2021; Hammarstrom et al., 2021; Miguez-Rey et al., 2022). Thus, we

compared side by side the neutralization potency of the combination of NA8 and NE12, used at equimolar concentrations (1:1), with that of six clinically approved antibodies used in paired combinations against the WA-1 strain and the Omicron sublineages BA.1 and BA.2 (Figure 2C). In agreement with previous reports (Cameroni et al., 2022; Cao et al., 2022b; Dejnirattisai et al., 2022; Planas et al., 2022; Wilhelm et al., 2021), all paired combinations were highly effective against WA-1, while only the combination of NA8 with NE12 retained high neutralization potency against Omicron BA.1. In contrast, no neutralization of Omicron BA.1 was detected with REGN-10933 in combination with REGN-10987, or with LY-CoV555 in combination with LY-CoV016, whereas the combination of COV2-2196 and COV2-2130 showed neutralizing activity that was more than 10-fold lower compared with that of the NA8-NE12 combination. Against the BA.2 sublineage, the NA8-NE12 combination was again the most potent, but a strong neutralization was also observed with the COV2-2130/COV2-2196 combination. Against the most recent variants, BA.2.12.1 and BA.4, the NA8-NE12 combination retained neutralizing activity at low nanomolar concentrations, as did the REGN-10933/REGN-10987 combination, while COV2-2130/COV2-2196 was the most potent combination and LY-CoV555/LY-CoV016 was ineffective (Figure 2C). Neutralization curves for the four paired combinations against the four Omicron sublineages are shown in Figures 2D–2G. In addition, we found that the combination of NA8 with NE12 was extremely potent against the original North American founder strain WA-1, the Alpha, Beta, and Delta variants, with IC<sub>50</sub> values between 0.5 and 5 ng/mL (Figure 2H). These results suggest that NA8 and NE12, when used in combination, are one of the most broad and potent antibody pairs with picomolar or low nanomolar neutralizing activity against the major SARS-CoV-2 variants of concern. Based on these results, NA8 and NE12 were selected for further characterization and preclinical testing. Complete neutralization curves for each of these two mAbs against all the viral variants tested are shown in Figures 2I and 2J. The neutralizing activity of our mAbs was also tested using a live virus neutralization assay against the early WA-1 isolate and the Beta variant (Figure S5A). This assay was less sensitive than the pseudovirus assay, a finding already reported by other authors (Zost et al., 2020a). However, the neutralization profile was similar, as

**Figure 2. Neutralizing activity of 18 monoclonal antibodies derived from convalescent COVID-19 patients and seven clinically approved monoclonal antibodies against different SARS-CoV-2 variants**

- (A) Heatmap of pseudovirus neutralization activity of 18 mAbs derived from convalescent COVID-19 patients. IC<sub>50</sub> values (μg/mL) are shown for neutralization of SARS-CoV-2 pseudoviruses bearing spike proteins from the USA/WA1/2020 isolate (WA-1, lineage A), the Alpha variant, Beta variant, Delta variant, and Omicron BA.1, BA.2, BA.4, and BA.2.12.1 sublineages. The color-coded legend of IC<sub>50</sub> ranges is indicated in (C).
- (B) Neutralizing activity of seven clinically approved mAbs, including REGN-10933, REGN-10987, LY-CoV555, LY-CoV016, COV2-2130, COV2-2196, and S309 (sotrovimab), against the same SARS-CoV-2 variants as in (A).
- (C) Neutralizing activity of mAbs NA8 and NE12 and six clinically approved mAbs used in paired combinations against the SARS-CoV-2 WA-1 strain and the Omicron BA.1, BA.2, BA.4, and BA.2.12.1 sublineages.
- (D) Neutralization curves of mAbs NE12 and NA8 and six clinically approved mAbs used in paired combinations against the Omicron BA.1 sublineage.
- (E) Neutralization curves of mAbs NE12 and NA8 and six clinically approved mAbs used in paired combinations against the Omicron BA.2 sublineage.
- (F) Neutralization curves of mAbs NE12 and NA8 and six clinically approved mAbs used in paired combinations against the Omicron BA.4 sublineage.
- (G) Neutralization curves of mAbs NE12 and NA8 and six clinically approved mAbs used in paired combinations against the Omicron BA.2.12.1 sublineage.
- (H) Neutralization curves of mAbs NE12 and NA8 used in combination against all major SARS-CoV-2 variants of concern.
- (I) Neutralization curves of mAb NA8 against the major SARS-CoV-2 variants of concern.
- (J) Neutralization curves of mAb NE12 against the major SARS-CoV-2 variants of concern. Results are the average of two or three independent experiments performed in duplicate using a pseudovirus assay. Values represent mean ± SD. The dotted horizontal lines indicate the IC<sub>90</sub> and IC<sub>50</sub>.

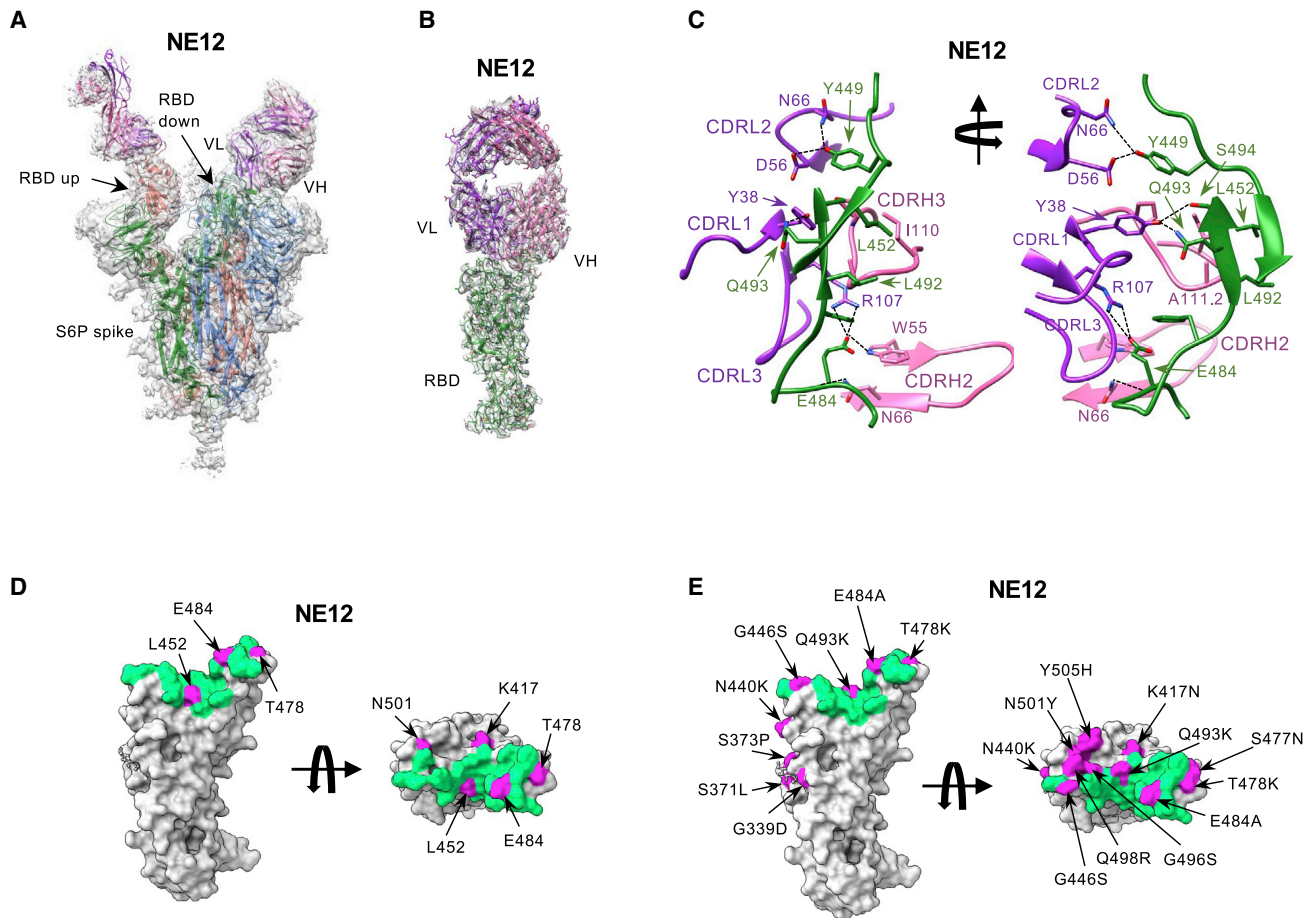


**Figure 3. Cryo-EM structures of the Fab fragment of neutralizing monoclonal antibody NE12 in complex with a stabilized SARS-CoV-2 spike protein trimer**

(A) Cryo-EM map of Fab NE12 in complex with the SARS-CoV-2 S-6P spike trimer with docked spike and Fab atomic models. The heavy and light chains of the mAb are colored in pink and purple, respectively. Spike protomers are colored individually. The Fab fragment binds the receptor-binding domain (RBD) in both the up and down positions.

(B) Local refinement of a region containing one RBD with bound Fab resolved atomic details of the RBD-NE12 interactions.

(C) Ribbon diagram of the RBD/NE12 contact interface. Coloring is as in panel (B). Only the complementarity-determining regions (CDRs) and RBD fragments participating in the interaction are shown for clarity. Key residues are shown in stick representation. Dashed lines represent salt bridges and hydrogen bonds.

(D and E) Surface representation of the RBD with the epitope of NE12 colored in green. Residues mutated in B.1.1.7/Alpha, B.1.617.2/Delta, and B.1.351/Beta (D) or Omicron BA.1 sublineage (E) variants of concern are colored in magenta. The antibody residues are numbered according to the IMGT (<http://www.imgt.org>) (Giudicelli et al., 2005).

shown by a strong correlation between the results obtained in the two assays (Figure S5B).

### Structural analysis of antibodies NE12 and NA8

To gain structural insight into the interactions of antibodies NE12 and NA8 with the SARS-CoV-2 spike glycoprotein, we obtained cryo-EM reconstructions of Fab NE12 and Fab NA8 bound to a stabilized spike trimer (S-6P) at nominal resolutions of 3.1 Å and 2.9 Å, respectively (Table S4; Figures S6–S9). In both structures, Fabs were observed bound to each of the three RBDs of the spike irrespectively of whether it assumed the up or down position (Figures 3A and 4A). The Fab-RBD interface was poorly resolved in the two consensus maps due to conformational variability of the S1 subunit of the spike (Figures S7 and S9). There-

fore, we performed signal subtraction and focused refinement of the region that included the RBD in the down position with the bound Fab and the proximal N-terminal domain. This improved the local resolution to 3.4 Å (NE12 complex) and 3.5 Å (NA8 complex), allowing detailed structural analysis of the Fab-RBD interactions (Figures 3B, 3C, 4B, 4C, S10, and S11).

Fab NE12 is positioned nearly parallel to the longest dimension of the RBD and interacts with the face of the receptor-binding ridge (Figures 3B and 3C). The interaction buries 874 Å<sup>2</sup> of the Fab surface area, split nearly equally between the heavy (465 Å<sup>2</sup>) and light (409 Å<sup>2</sup>) chains, and 828 Å<sup>2</sup> of the RBD surface area. The 17-residue-long CDR3 of the heavy chain (CDRH3) and the CDR1 of the light chain (CDRL1) straddle the receptor-binding ridge, while the CDRL3 and CDRH2 interact

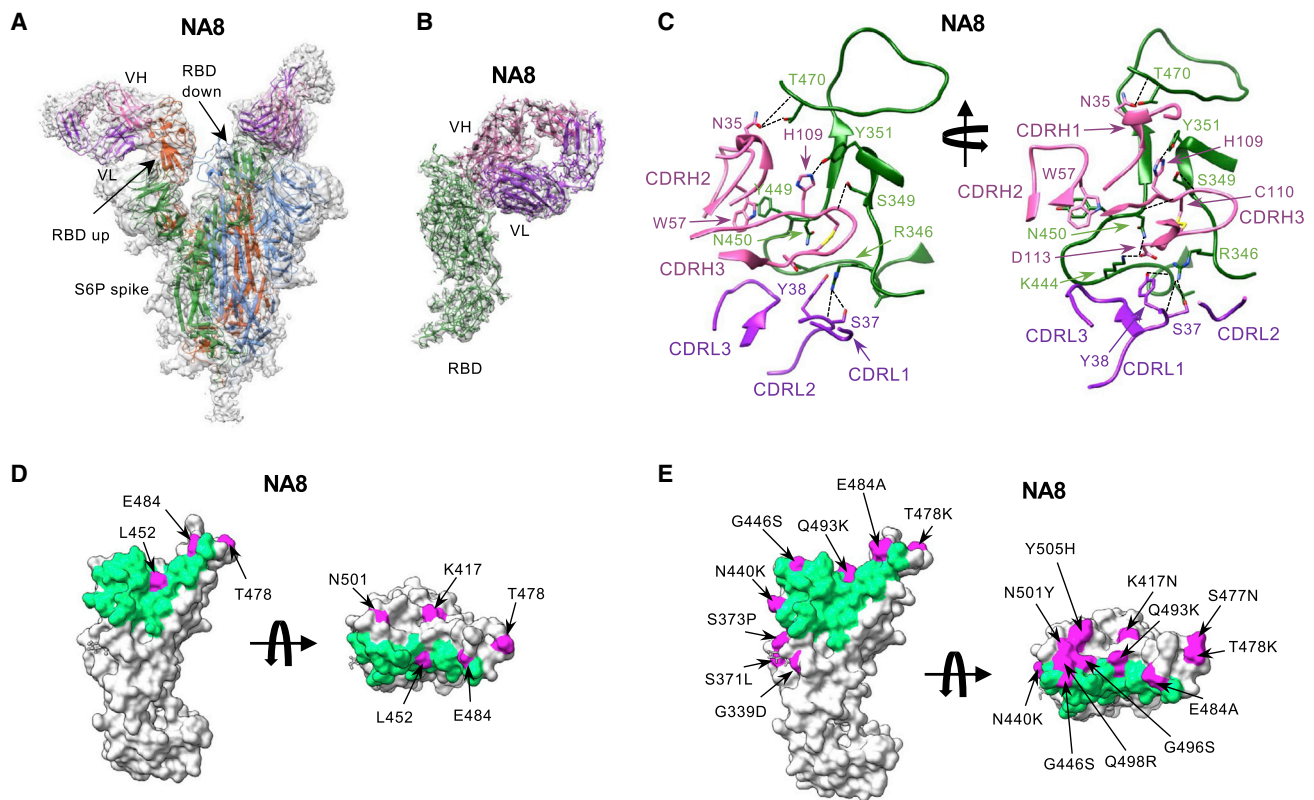


**Figure 4. Cryo-EM structures of the Fab fragment of neutralizing monoclonal antibody NA8 in complex with a stabilized SARS-CoV-2 spike protein trimer**

(A) Cryo-EM map of Fab NA8 in complex with the SARS-CoV-2 S-6P spike trimer with docked spike and Fab atomic models. The heavy and light chains of the mAb are colored in pink and purple, respectively. Spike protomers are colored individually. The Fab fragment binds the receptor-binding domain (RBD) in both the up and down positions.

(B) Local refinement of a region containing one RBD with bound Fab resolved atomic details of the RBD-NA8 interactions.

(C) Ribbon diagram of the RBD/NA8 contact interface. Coloring is as in (B). Only the complementarity-determining regions (CDRs) and RBD fragment participating in the interaction are shown for clarity. Key residues are shown in stick representation. Dashed lines represent salt bridges and hydrogen bonds.

(D and E) Surface representation of the RBD with residues mutated in the B.1.1.7/Alpha, B.1.617.2/Delta, and B.1.351/Beta (D) or Omicron BA.1 sublineage (E) variants of concern are colored in magenta.

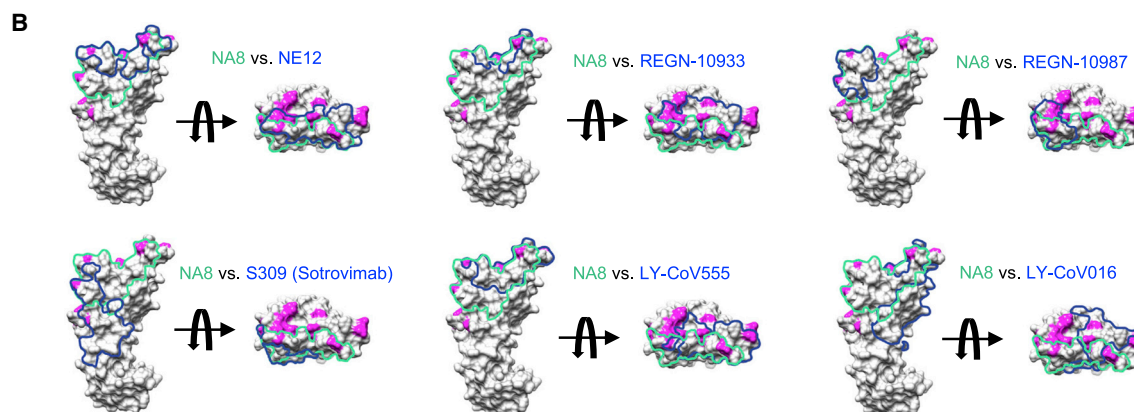
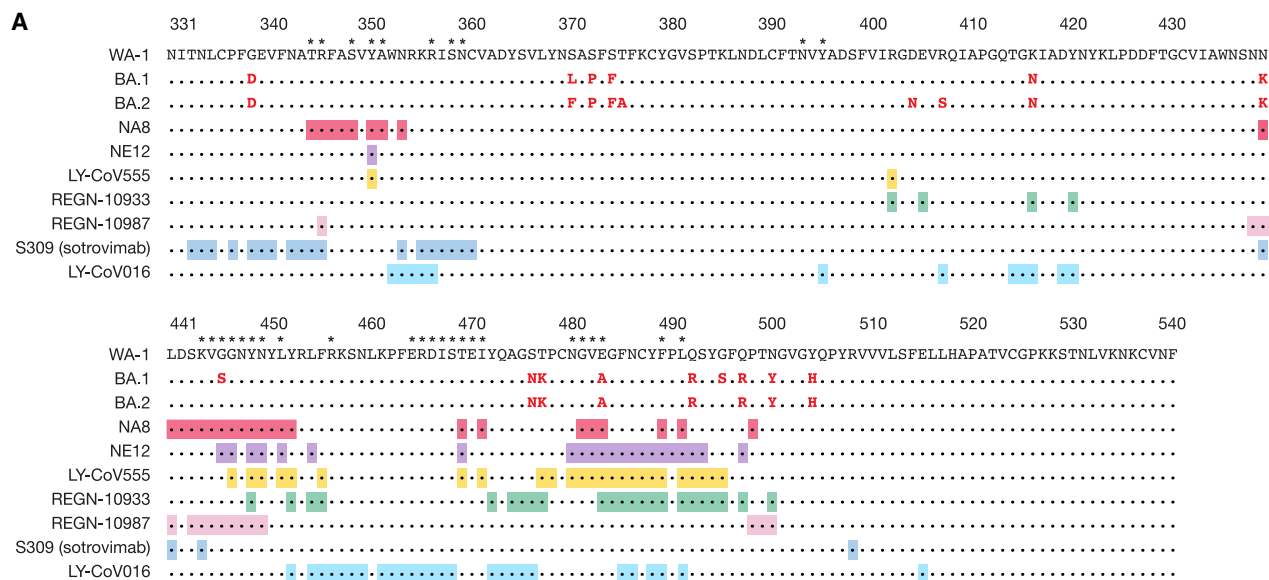
The antibody residues are numbered according to the IMGT (<http://www.imgt.org>) (Giudicelli et al., 2005).

with the tip of the RBD (Figure 3C). The CDRH1 does not contribute to the paratope and is disordered, while the CDRL2 interacts with the region of the receptor-binding ridge distant from the tip. The location of the epitope, the ability to bind the RBD both in the up and down positions, and the long CDRH3 allowed the categorization of NE12 as a class 2 antibody as defined by Barnes et al. (Barnes et al., 2020). Based on the alternative classification system of Hastie et al. (Hastie et al., 2021), NE12 belongs to group RBD-2b.2. Its epitope overlaps with those of mAbs LY-CoV555 (Jones et al., 2021) and REGN-10933 (Hansen et al., 2020), as well as with the ACE2 receptor footprint (Shang et al., 2020), indicating that NE12 directly blocks the spike-receptor interaction (Figure S12). This mechanism was confirmed by binding competition studies on ACE2-expressing cells (Figure S13A). Residues mutated in the B.1.1.7/Alpha and B.1.617.2/Delta variants are located outside or at the periphery of the NE12 epitope, thus allowing for a potent neutralization of these variants (Figure 3D). In contrast, the E484K mutation of

B.1.351/Beta results in clashes with CDRH2 and CDRL3 residues, compromising the neutralizing activity. Likewise, multiple replacements in the Omicron BA.1 sublineage RBD receptor-binding ridge can affect NE12-spike interactions (Figure 3E).

Similar to Fab NE12, Fab NA8 shows extensive contacts with the receptor-binding ridge, but this antibody binds to a distinct epitope along the outer side of the RBD distal from the tip (Figures 4B and 4C). While NA8 interacts with the periphery of the receptor-binding ridge (typical of class 2 antibodies), its epitope is shifted toward the glycosylated Asn<sup>343</sup> (typical of class 3 antibodies), although it does not include this residue or the glycan. Thus, NA8 displays characteristics of both Barnes class 2 and class 3 antibodies (Barnes et al., 2020), while the Hastie classification system (Hastie et al., 2021) categorizes it as an RBD-4 mAb. Analysis of contact surfaces reveals a moderate overlap between the NA8 epitope and the ACE2-binding interface of the RBD (Figure S13B). Accordingly, binding competition studies on ACE2-expressing cells provided evidence that NA8





**C**

Antibody	Characteristic of antibody-encoding genes				Fab $K_d$ (nM)	In vitro neutralization $IC_{50}$ ( $\mu$ g/ml) <sup>1</sup>		Epitope class <sup>2</sup>	Reference
	IgHV (% SHM)	CDR3H length (aa)	IgLV (% SHM)	CDRL3 length (aa)		WA-1	Omicron		
NE12	VH1-2 (2)	17	VK3-11 (0.4)	10	0.61	0.003	6.500	2/RBD-2b.2	This study
NA8	VH3-33 (5)	16	VK1-39 (0.8)	9	0.46	0.008	0.004	2&3/RBD-4	This study
REGN-10933	VH3-11 (1.4)	13	VK1-33 (1.1)	9	3.4	0.002	>10	1/RBD-2a	Hansen et al. 2020
REGN-10987	VH3-30 (1.4)	13	VL2-14 (2.4)	10	45.2	0.009	>10	3/RBD-5	Hansen et al. 2020
LY-CoV555	VH1-69 (0.3)	18	VK1-39 (0.7)	9	1.45	0.003	>10	2/RBD-2b.2	Jones et al. 2021
LY-CoV016	VH3-66 (1)	13	VK1-39 (0.4)	11	2.5	0.019	>10	1/RBD-1	Shi et al. 2020
S309	VH1-8 (2.8)	20	VK3-20 (2.5)	8	2.6	0.475	0.371	3/RBD-5	Pinto et al. 2020
CoV2-2196	VH1-58 (1)	16	VK3-20 (0.7)	10	NA <sup>3</sup>	0.001	0.139	1/ND	Zost et al. 2020
CoV2-2130	VH3-15 (1.4)	22	VK4-1 (1.3)	8	NA	0.001	0.663	2/ND	Zost et al. 2020

(legend on next page)

reduced the interaction between the spike trimer and ACE2 by 90% (Figure S13A). The interaction buries 981 Å<sup>2</sup> of the Fab surface area, with the heavy chain responsible for most contacts (642 Å<sup>2</sup>) and 990 Å<sup>2</sup> of the RBD surface area. The CDRH3 forms a long loop positioned along the side of the RBD, whereas the CDRH1 and CDRH2 contact the central region of the receptor-binding ridge. The CDRL1 and CDRL2 interact with the side of the RBD, while the CDRL3 contacts the loop formed by RBD residues 444–447. Of the residues mutated in the variants of concern, only L452 is part of the NA8 epitope (Figure 4D), which can explain the reduced neutralization of B.1.617.2/Delta. Noteworthy, all the B.1.351/Beta and Omicron BA.1 mutations fall outside the NA8 epitope or are located at its periphery (Figures 4E and 5A), which is consistent with the high neutralization potency of NA8 against these variants. Comparison of the NA8 footprint with those of NE12 and several clinically approved mAbs (Figure 5B) shows that the NA8 epitope is partially overlapping but distinct from the epitopes of REGN-10933, REGN-10987, S309 (sotrovimab), LY-CoV555, and LY-CoV016. Of note, BA.1 and BA.2 share the same mutations in the regions targeted by NA8 except for Ser446 of BA.1, which is reverted to a glycine in the BA-2 sublineage (Figure 5A); this explains the ability of NA8 to efficiently neutralize both sublineages.

In summary, based on their binding affinity, neutralization potency, and breadth, NE12 and NA8 provide a pair of potent complementary mAbs for potential clinical use (Figure 5C).

### Antibodies NE12 and NA8 protect hamsters from SARS-CoV-2 infection

Next, we tested the *in vivo* prophylactic efficacy of the two selected mAbs, NE12 and NA8, in the golden Syrian hamster model, which closely mimics the severity of the disease in humans (Baum et al., 2020a; Imai et al., 2020). A total of 80 male hamsters were used for these experiments; each study group included 10 hamsters. The animals were inoculated with mAbs at two concentrations (12 and 4 mg/kg) via intraperitoneal injection 24 h before intranasal challenge with 4.5 log<sub>10</sub> TCID<sub>50</sub> of SARS-CoV-2 WA-1 or B.1.351/Beta (Figure 6A). An isotype-matched (IgG1) irrelevant mAb, the anti-HIV-1 VRC01, was included as a control at 12 mg/kg. Based on the *in vitro* neutralization results, both NA8 and NE12 were tested against the WA-1 strain (Figures 6B, 6D, and 6E), while only NA8 was tested against the B.1.351/Beta variant (Figures 6C, 6F, and 6G). Animals treated with the control IgG1 lost, on average, 9% and 8% of body weight by day 5 after challenge with WA-1 and B.1.351, respectively (Figures 6B and 6C). In contrast, treatment with NE12 or NA8 significantly protected hamsters from weight loss induced by the two viral variants, although NA8 at 4 mg/kg against the B.1.351 virus showed a lesser degree of pro-

tection (Figure 6C). The protective effect of NE12 and NA8 was confirmed by viral load measurements in nasal turbinate and lung tissues on days 3 and 5 after inoculation (n = 5 per time point per group). In animals treated with NE12 or NA8 at either 12 or 4 mg/kg, the viral titers at day 3 post-infection with the WA-1 virus were significantly reduced in both tissues compared with controls; in the lungs, the virus became undetectable at day 5 post-infection (Figures 6D and 6E). Likewise, in animals infected with the B.1.351 variant, NA8 at both concentrations significantly reduced the viral titers in nasal turbinate and lung tissues at day 3 post-infection and completely suppressed viral replication in the lungs at day 5 (Figures 6F and 6G). Overall, these data demonstrate that NA8 exerted strong prophylactic protection *in vivo* from two antigenically distinct SARS-CoV-2 variants, and NE12 exerted strong prophylactic protection against SARS-CoV-2 WA-1 in a susceptible animal model, despite the relatively low antibody doses used.

### Antibodies NE12 and NA8 have therapeutic activity against SARS-CoV-2 in hamsters

To investigate the therapeutic activity of NE12 and NA8 against SARS-CoV-2, a total of 60 male hamsters, divided in six groups of 10 animals each, were utilized for a therapeutic study. Three groups of animals were infected intranasally with the original strain, WA-1, and three groups with the B.1.351/Beta variant (4.5 log<sub>10</sub> TCID<sub>50</sub> per animal). The therapeutic efficacy of NE12 or NA8 (each at 12 mg/kg) was evaluated by administering the antibodies via the intraperitoneal route 24 h after intranasal challenge (Figure 7A). This is a very stringent model given the extremely rapid kinetics of replication of SARS-CoV-2. The IgG1 isotype control mAb VRC01 (12 mg/kg) was tested in parallel as a control. Five hamsters per group were sacrificed at day 3 post-infection for tissue viral load measurements, while the remaining 5 animals were weighed daily until day 11. No significant differences in weight loss were observed among the three groups of hamsters infected with WA-1 (Figure 7B). In contrast, NA8 significantly reduced the weight loss caused by infection with the B.1.351/Beta variant, which remained below 5% of the initial body weight throughout the observation period in contrast with the marked loss (nearly 15%) seen in the control group (Figure 7C). Analysis of viral titers in nasal turbinate and lung tissues showed a significant reduction in both NE12- and NA8-treated animals infected with WA-1, despite a wide data distribution in animals treated with NE12 (Figures 7D and 7E). The serum concentrations of NA8 and NE12 were measured on day 3 after infection. The three animals in the NE12/WA-1 group that showed high viral titers in nasal turbinates and lungs had low to undetectable antibody levels in serum (Figure S14), which may reflect a failure in intraperitoneal injection, as reported

### Figure 5. Comparison of binding epitopes, genetic characteristics, and neutralizing activity of NA8 and NE12 with clinically approved monoclonal antibodies

- (A) Amino acid sequences of the receptor-binding domain (RBD) of Omicron sublineages BA.1 and BA.2 with mutations colored in red compared with the sequence of the original North American founder strain WA-1 (GenBank: MN985325); the asterisks indicate residues that contact the ACE receptor. The binding epitopes of different mAbs are presented below and highlighted in different colors.
- (B) Surface representation of the RBD with the epitopes of NA8 (green line) and NE12 or clinically approved monoclonal antibodies (blue line) highlighted. Surface areas corresponding to the RBD residues mutated in the Omicron BA.1 sublineage are colored in magenta.
- (C) Characteristics of NA8 and NE12 in comparison with clinically approved mAbs against SARS-CoV-2.

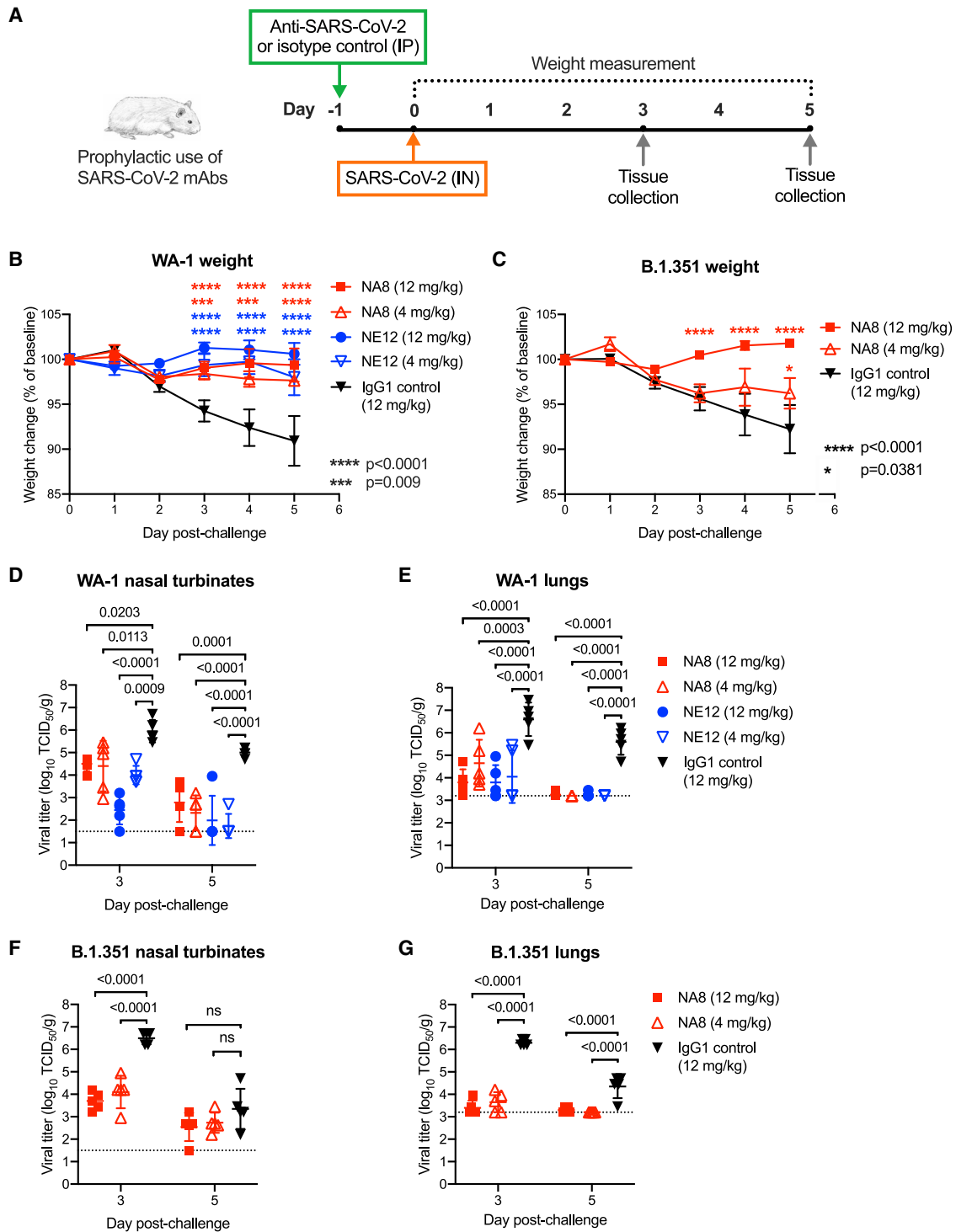


**Figure 6. Prophylactic efficacy of two neutralizing monoclonal antibodies, NE12 and NA8, against infection with SARS-CoV-2 in the golden Syrian hamster model**

(A) Design of the study. MAbs NE12 or NA8 were administered intraperitoneally (IP) at the dose of 12 or 4 mg/kg. Control animals received an anti-HIV-1 IgG1 (VRC01) at 12 mg/kg. One day later, each group of 10 animals was challenged with  $10^{4.5}$  TCID<sub>50</sub> of SARS-CoV-2 WA-1 or B.1.351 instilled intranasally (IN). The animal weight was monitored daily (days 0–3: n = 10 per group; days 4, 5: n = 5 per group) as an indicator of disease progression. Tissues were collected for virus quantification at 3 and 5 days after challenge (n = 5 per group per time point).

(legend continued on next page)

by other authors (Starr et al., 2021). In hamsters infected with B.1.351, treatment with NA8 induced a significant reduction in viral titers in both nasal turbinate and lung tissues, while, as expected, NE12 was ineffective (Figures 7F and 7G). Altogether, these results demonstrate that both NE12 and NA8 exerted strong therapeutic effects against sensitive SARS-CoV-2 strains in a suitable preclinical model.

## DISCUSSION

In this study, we report the generation of a panel of potent human mAbs capable of neutralizing highly diverse and transmissible SARS-CoV-2 variants of concern. Within this panel, we selected two mAbs, NA8 and NE12, as promising candidates for clinical use. The most important observation from this work is that, despite the substantial mutation of this virus, the immune system has the potential to develop RBD-directed antibodies that are capable of potent neutralization and yet retain a broad spectrum of action to overcome the continuous immune escape of evolving SARS-CoV-2 variants of concern. NA8 and NE12 have distinctive and complementary properties. NA8 features a very broad spectrum of action with ultrapotent activity, at low picomolar concentrations, against difficult-to-neutralize variants of concern, namely, Beta and Omicron sublineages BA.1 and BA.2, and at nanomolar concentrations against the most recently emerged BA.2.12.1 and BA.4. The Beta variant is particularly resistant to neutralization, and indeed very few effective mAbs are currently available (Wang et al., 2021; Wibmer et al., 2021). Likewise, the most widely clinically used mAbs, including sotrovimab (Cameroni et al., 2022; Cao et al., 2022b; Cathcart et al., 2021), have reduced or no neutralizing activity against the recently emerged Omicron variants. The Omicron BA.2 sublineage, which rapidly replaced the previously dominant BA.1 in many countries, was found to be resistant to 17 out of 19 neutralizing mAbs tested, including sotrovimab, which had retained some activity against BA.1, indicating that mAbs react in a different manner against the Omicron sublineages (Iketani et al., 2022). Among the mAbs currently approved for clinical use that were evaluated in our study, only AZD1061/COV2-2130 (cilgavimab) showed strong neutralizing activity against the BA.2 and BA.2.12.1 sublineages, but its efficacy against the BA.1 sublineage was markedly reduced. Very recently, FDA granted emergency use authorization for a new mAb, LY-CoV1404 (bebtelovimab), which has an *in vitro* potency against Omicron comparable to that of NA8 (Westendorf et al., 2022), but this antibody was not available for side-by-side comparison with our mAbs.

The structural basis for the breadth of neutralization of NA8, which has mixed features of both Barnes class 2 and class 3 antibodies, lies in the high conservation of its binding epitope, as

revealed by cryo-EM analysis. The NA8 epitope is distinct from those of other mAbs hitherto reported in that, despite including a portion of the receptor-binding ridge, it is shifted toward the outer side of the RBD, allowing the antibody to “sidestep” the residues that are mutated in the Beta and Omicron variants. The second mAb described herein, NE12, has features of a Barnes class 2 antibody and binds to an epitope that largely overlaps with the ACE2 receptor footprint on the RBD.

NA8 and NE12 have a complementary neutralization spectrum, and indeed, when used in combination, they showed potent activity against all the major SARS-CoV-2 variants tested. Among the clinically approved mAbs tested, only the combination of COV2-2130 and COV2-2196 showed a comparable breadth. Although NA8 and NE12 bind to partially overlapping epitopes, as is the case for LY-CoV555 and LY-CoV016, their neutralization potency was not affected when used in combination. Although antibodies targeting overlapping epitopes can displace one another, particularly when their association rate is similar, it has been shown that the displacement is reversible if sufficient time is allowed to reach a state of equilibrium (Abdiche et al., 2017). This model is consistent with our experimental observations whereby an equimolar combination of NA8 and NE12 neutralized all viral variants with the same potency as that of the most effective of the two antibodies.

Considering the reduced efficacy of current vaccines and the complete loss or reduced neutralizing activity of most clinically approved antibodies to the Omicron variants (Aggarwal et al., 2021; Bowen et al., 2022a; Bruel et al., 2022; Cameroni et al., 2022; Cao et al., 2022a; Cao Y. et al., 2022b; Cathcart et al., 2021; Cele et al., 2022; Dejnirattisai et al., 2022; Doria-Rose et al., 2021; Hachmann et al., 2022; Iketani et al., 2022; Mannar et al., 2022; Planas et al., 2022; Qu et al., 2022; Shrestha et al., 2022; Takashita et al., 2022; Wilhelm et al., 2021; Zhou et al., 2022), the isolation of new antibodies capable of blocking a broad spectrum of emergent SARS-CoV-2 variants of concern is important for future therapeutic and preventive strategies. Due to the high degree of conservation of its binding epitope, our mAb NA8 has the potential to neutralize new variants that will continue to emerge over time, especially from areas of the world with low vaccination rates. Corroborating the potential clinical usefulness of our antibodies, the *in vitro* neutralization potency of NE12 and NA8 was confirmed in a hamster model *in vivo*, in which both mAbs exhibited remarkable prophylactic and therapeutic efficacy against the original WA-1 strain and the Beta variant at relatively low doses.

In summary, the identification of potent, broadly neutralizing human antibodies against SARS-CoV-2 variants of concern that resist neutralization by most mAbs, such as the Beta and the Omicron sublineages BA.1 and BA.2, is critical for creating

(B and C) Body weight changes (means  $\pm$  SE) from baseline in hamsters that received neutralizing mAbs at different doses or isotype control (IgG) after challenge with (B) WA-1 or (C) B.1.351 SARS-CoV-2 strains.

(D–G) Viral titers in (D) nasal turbinate and (E) lung tissues at days 3 and 5 post-infection with (F) WA-1 or (G) the B.1.351 variant, as determined using an assay to quantify the TCID<sub>50</sub> of infectious virus. Individual titers and means  $\pm$  SD are shown for each group. Dashed lines indicate the limit of detection of the assay. Statistical comparisons of weight changes between treatment groups were performed using a repeated-measures mixed-effects model with Tukey’s multiple-comparison test (B and C). Comparisons of the viral titers between groups were performed using two-way analysis of variance (ANOVA) with Tukey’s multiple-comparison test. p values between groups treated with neutralizing mAbs and isotype control are indicated. p > 0.05, not significant (ns); \*p = 0.0381; \*\*\*p = 0.0009; \*\*\*\*p < 0.0001.

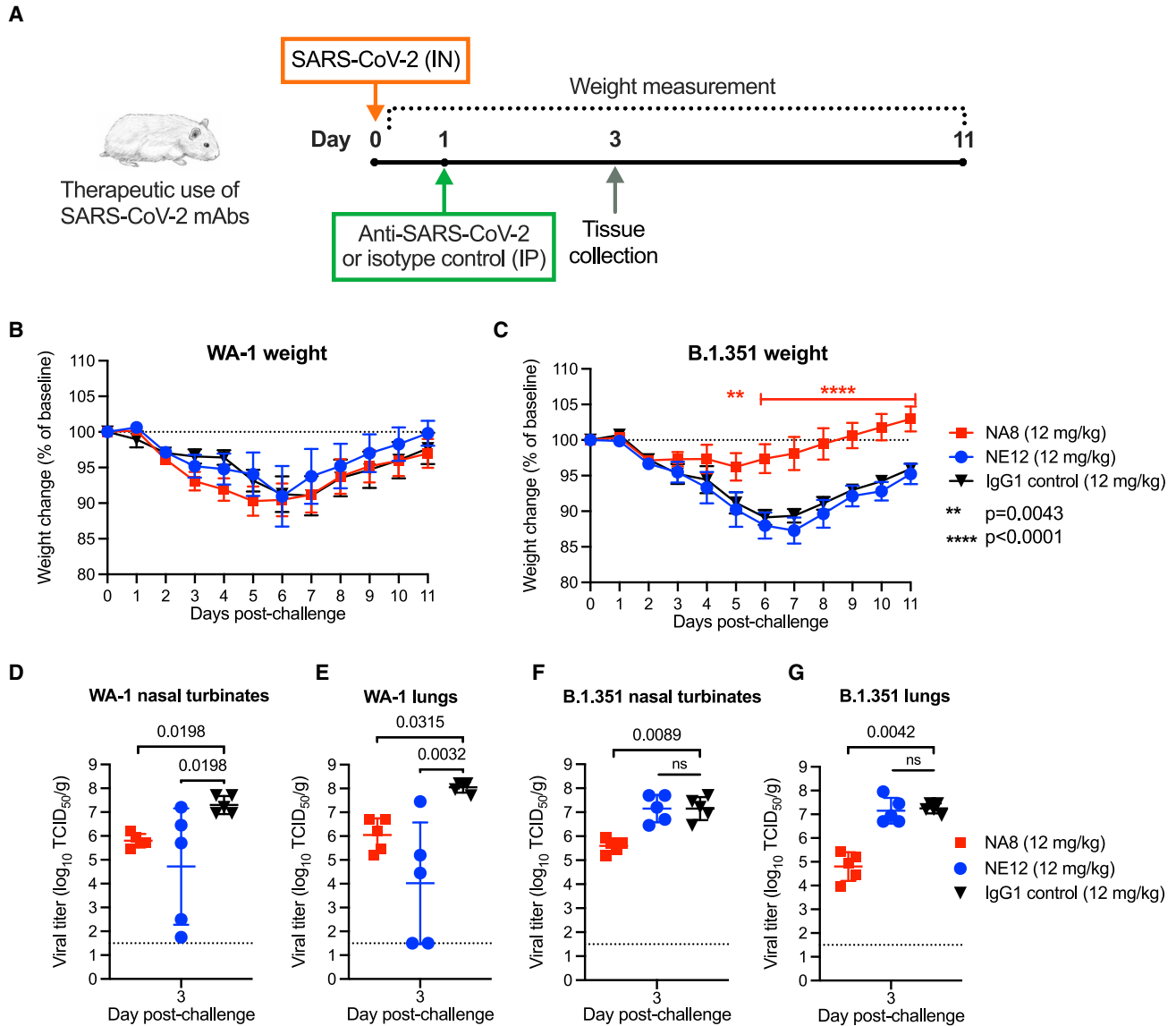


**Figure 7. Therapeutic efficacy of two neutralizing mAbs, NE12 and NA8, against SARS-CoV-2 in the golden Syrian hamster model**

(A) Design of the study. Each group of 10 animals was first challenged with  $10^{4.5}$  TCID<sub>50</sub> of SARS-CoV-2 WA-1 or B.1.351/Beta, instilled intranasally (IN). Twenty-four hours later, the animals were injected intraperitoneally (IP) with mAbs NE12 or NA8 at the dose of 12 mg/kg. Control animals received an anti-HIV-1 IgG1 (VRC01) at 12 mg/kg. The animal weight was monitored daily as an indicator of disease progression (days 0–2: n = 10 per group; days 3–11: n = 5 per group, except for the WA-1/NE12 group (days 6–11: n = 3 due to a technical issue). Tissues were collected at day 3 after challenge for virus quantification (n = 5 per group).

(B and C) Body weight changes (means ± SE) from baseline in hamsters that were challenged with SARS-CoV-2 (B) WA-1 or (C) B.1.351/Beta.

(D–G) Quantification of viral titers at day 3 post-challenge in (D) nasal turbinate and (E) lung tissues of animals infected with WA-1 or in (F) nasal turbinate and (G) lung tissues of animals infected with the B.1.351/Beta variant, as determined using an assay to quantify the TCID<sub>50</sub> of infectious virus. Individual titers and means ± SD are shown for each group. Dashed lines indicate the limit of detection of the assay. Statistical comparisons of weight changes between treatment groups were performed using a repeated-measures mixed-effects model with Tukey's multiple-comparison test. Comparisons of viral titers between the treatment groups were performed using the non-parametric Kruskal-Wallis test with a Benjamini, Krieger, and Yekutieli false discovery test. p values between groups treated with neutralizing mAbs and isotype control are indicated. p > 0.05, not significant (ns); \*\*p = 0.0043; \*\*\*\*p < 0.0001.

an arsenal of therapeutic antibodies with high potency against both present and future variants of concern that will continue to emerge because of the sustained worldwide spread of this virus, leading to escape from current prophylactic and therapeutic interventions.

#### Limitations of the study

Although we documented the *in vivo* protective and therapeutic efficacies of our mAbs, NA8 and NE12, in the hamster model against two different SARS-CoV-2 strains (WA-1 and Beta variant), we did not test them against other variants of concern

of global relevance such as the various Omicron sublineages. However, based on their *in vitro* neutralization activity, we could infer that our antibodies would be effective against these variants in the preclinical model, although physicochemical properties of our antibodies that were not addressed in this study can have a major influence on *in vivo* efficacy (Jain et al., 2017). Another limitation of this study is that most of the neutralization results were obtained using a pseudovirus-based assay that employs ACE2-transfected HEK293 cells as targets. However, this assay is widely used in the field and was shown to predict the *in vivo* neutralizing activity of mAbs, as also confirmed in this study.

## STAR★METHODS

Detailed methods are provided in the online version of this paper and include the following:

- **KEY RESOURCES TABLE**
- **RESOURCE AVAILABILITY**
  - Lead contact
  - Materials availability
  - Data and code availability
- **EXPERIMENTAL MODEL AND SUBJECT DETAILS**
  - Convalescent COVID-19 plasma donor selection, human samples, and lymphocyte isolation
- **METHOD DETAILS**
  - Live virus neutralization assay used to test COVID-19 convalescent patients
  - Human Fab antibody library construction
  - Expression and purification of recombinant SARS-CoV-2 spike protein trimers
  - Selection of specific Fab clones
  - Sequence analysis of S-2P-positive Fab clones
  - Expression and purification of Fab and IgG
  - ELISA assays
  - Surface plasmon resonance (SPR)
  - Pseudotype neutralization assay
  - Live virus neutralization assay
  - Cryo-EM specimen preparation and data collection
  - Single particle analysis of cryo-EM data
  - Atomic model generation
  - Prophylactic and therapeutic studies in the hamster model
- **QUANTIFICATION AND STATISTICAL ANALYSIS**
  - Statistical analysis

## SUPPLEMENTAL INFORMATION

Supplemental information can be found online at <https://doi.org/10.1016/j.celrep.2022.111528>.

## ACKNOWLEDGMENTS

We wish to thank John R. Mascola, Kizzmekia S. Corbett, Nicole Doria-Rose, Lingshu Wang, Kevin Carlton, and the Vaccine Production Program of the Vaccine Research Center (VRC), NIAID, NIH, for providing mAbs REGN-10933, REGN-10987, LY-CoV555, LY-CoV016, S309, and VRC01, plasmids to express the SARS-CoV-2 stabilized S-2P and S-6P spike trimers, membrane-bound spike proteins from various SARS-CoV-2 strains,

the lentivirus backbone pCMV DR8.2, and human TMPRSS2; Michael Farzan for providing 293-ACE2 cells; Craig Martens for sequencing the SARS-CoV-2 stocks; and the staff of the NIAID Comparative Medicine Branch for animal study support. We also wish to thank Dr. Anthony S. Fauci, Dr. Steven Holland, and Dr. Jeffrey I. Cohen for critically reading the manuscript and for their helpful suggestions. This work was supported by the Intramural Research Program of the National Institute of Allergy and Infectious Diseases (NIAID), National Institutes of Health (NIH), and by the Intramural Research Program of the VRC, NIAID, NIH. This work was also supported by Federal funds from the NIAID, NIH, under Contract No. HHSN272201800013C, by Federal funds from the Frederick National Laboratory for Cancer Research (FNLCR), NIH, under Contract HHSN261200800001 (Y.T., T.S.). Cryo-EM datasets were collected at the National CryoEM Facility (NCEF) of the National Cancer Institute (NCI) with the support of the NCI National Cryo-EM Facility at the FNLCR under contract HSSN26120080001E. Chimera was developed by the Resource for Biocomputing, Visualization, and Informatics at the University of California, San Francisco, with support from NIH P41-GM103311. The Frederick Research Computing Environment (FRCE) high-performance computing cluster was used for processing cryo-EM datasets. R.G. and M.R.H. performed this work as employees of Laulima Government Solutions, LLC, while E.P. performed this work as an employee of Tunnell Government Services. The content of this publication does not necessarily reflect the views or policies of the US Department of Health and Human Services (DHHS) or of the institutions and companies affiliated with the authors.

## AUTHOR CONTRIBUTIONS

Z.C. and P.F. conceived the research and designed the study, and Z.C., P.Z., Y.M., Y.T., D.H.M., P.D.K., H.J.A., U.J.B., P.L., and P.F. designed experiments, and K.W., V.D.G., and H.J.A. contributed to donor recruitment and blood sample collection, and Z.C. generated Fab libraries and cloned monoclonal antibodies, and H.N. and A.P. contributed to plasmid DNA preparation and tissue culture for IgG production, and B.Z. produced antibodies, and P.Z. and P.L. produced pseudoviruses and performed pseudovirus neutralization assays, and E.P., R.G., M.R.H., Y.M., and C.S. performed live virus neutralization assays, and L.F.B. and D.H.M. performed binding assays and data analysis, and Y.M. and C.S. performed animal studies, and Y.M. and U.J.B. analyzed results, and N.L.G. and R.F.J. generated and characterized the SARS-CoV-2 stocks for the animal studies, and A.S.O. expressed, purified, and provided S-6P spike for cryo-EM structural analysis, and T.S. carried out specimen preparation for cryo-EM experiments, and Y.T. performed cryo-EM experiments and with P.D.K. performed data analysis and interpretation of the cryo-EM structures, and P.F. with Z.C., Y.T., U.J.B., and P.L. wrote the manuscript with all authors providing revisions and comments, and P.F. provided supervision for the entire project.

## DECLARATION OF INTERESTS

Z.C., P.F., K.W., P.Z., P.L., U.J.B., and Y.M. are named on an unpublished patent application filed by the National Institutes of Health related to the work described herein.

Received: April 26, 2022

Revised: July 29, 2022

Accepted: September 28, 2022

Published: September 30, 2022

## REFERENCES

Abdiche, Y.N., Yeung, A.Y., Ni, I., Stone, D., Miles, A., Morishige, W., Rossi, A., and Strop, P. (2017). Antibodies targeting closely adjacent or minimally overlapping epitopes can displace one another. *PLoS One* 12, e0169535. <https://doi.org/10.1371/journal.pone.0169535>.

- Afonine, P.V., Klaholz, B.P., Moriarty, N.W., Poon, B.K., Sobolev, O.V., Terwilliger, T.C., Adams, P.D., and Urzhumtsev, A. (2018). New tools for the analysis and validation of cryo-EM maps and atomic models. *Acta Crystallogr. D Struct. Biol.* 74, 814–840. <https://doi.org/10.1107/S2059798318009324>.
- Aggarwal, A., Stella, A.O., Walker, G., Akerman, A., Milogiannakis, V., Brilot, F., Amatayakul-Chantler, S., Roth, N., Coppola, G., Schofield, P., et al. (2021). SARS-CoV-2 Omicron: evasion of potent humoral responses and resistance to clinical immunotherapeutics relative to viral variants of concern. Preprint at medRxiv. <https://doi.org/10.1101/2021.12.14.21267772>.
- Andreano, E., Nicastrì, E., Paciello, I., Pileri, P., Manganaro, N., Piccini, G., Manenti, A., Pantano, E., Kabanova, A., Troisi, M., et al. (2021). Extremely potent human monoclonal antibodies from COVID-19 convalescent patients. *Cell* 184, 1821–1835.e16. <https://doi.org/10.1016/j.cell.2021.02.035>.
- Barbas, C.F., 3rd, Kang, A.S., Lerner, R.A., and Benkovic, S.J. (1991). Assembly of combinatorial antibody libraries on phage surfaces: the gene III site. *Proc. Natl. Acad. Sci. USA* 88, 7978–7982. <https://doi.org/10.1073/pnas.88.18.7978>.
- Barnes, C.O., Jette, C.A., Abernathy, M.E., Dam, K.M.A., Esswein, S.R., Gristick, H.B., Malyutin, A.G., Sharaf, N.G., Huey-Tubman, K.E., Lee, Y.E., et al. (2020). SARS-CoV-2 neutralizing antibody structures inform therapeutic strategies. *Nature* 588, 682–687. <https://doi.org/10.1038/s41586-020-2852-1>.
- Baum, A., Ajithdoss, D., Copin, R., Zhou, A., Lanza, K., Negron, N., Ni, M., Wei, Y., Mohammadi, K., Musser, B., et al. (2020a). REGN-COV2 antibodies prevent and treat SARS-CoV-2 infection in rhesus macaques and hamsters. *Science* 370, 1110–1115. <https://doi.org/10.1126/science.abe2402>.
- Baum, A., Fulton, B.O., Wloga, E., Copin, R., Pascal, K.E., Russo, V., Giordano, S., Lanza, K., Negron, N., Ni, M., et al. (2020b). Antibody cocktail to SARS-CoV-2 spike protein prevents rapid mutational escape seen with individual antibodies. *Science* 369, 1014–1018. <https://doi.org/10.1126/science.abd0831>.
- Bennett, R.S., Postnikova, E.N., Liang, J., Gross, R., Mazur, S., Dixit, S., Kocher, G., Yu, S., Georgia-Clark, S., Gerhardt, D., et al. (2021). Scalable, micro-neutralization assay for assessment of SARS-CoV-2 (COVID-19) virus-neutralizing antibodies in human clinical samples. *Viruses* 13. <https://doi.org/10.3390/v13050893>.
- Bowen, J.E., Sprouse, K.R., Walls, A.C., Mazzitelli, I.G., Logue, J.K., Franko, N.M., Ahmed, K., Shariq, A., Cameroni, E., Gori, A., et al. (2022a). Omicron BA.1 and BA.2 neutralizing activity elicited by a comprehensive panel of human vaccines. Preprint at bioRxiv. <https://doi.org/10.1101/2022.03.15.484542>.
- Bowen, J.E., Addetia, A., Dang, H., Stewart, C., Brown, J.T., Sharkey, W.K., Sprouse, K.R., Walls, A.C., Mazzitelli, I.G., Logue, J.K., et al. (2022b). Science, eabq0203. <https://doi.org/10.1126/science.abq0203>.
- Boyd, S.D., Gaëta, B.A., Jackson, K.J., Fire, A.Z., Marshall, E.L., Merker, J.D., Maniar, J.M., Zhang, L.N., Sahaf, B., Jones, C.D., et al. (2010). Individual variation in the germ-line Ig gene repertoire inferred from variable region gene rearrangements. *J. Immunol.* 184, 6986–6992. <https://doi.org/10.4049/jimmunol.1000445>.
- Bruel, T., Hadjadj, J., Maes, P., Planas, D., Seve, A., Staropoli, I., Guivel-Benhassine, F., Porrot, F., Bolland, W.H., Nguyen, Y., et al. (2022). Serum neutralization of SARS-CoV-2 Omicron sublineages BA.1 and BA.2 in patients receiving monoclonal antibodies. *Nat. Med.* 28, 1297–1302. <https://doi.org/10.1038/s41591-022-01792-5>.
- Cameroni, E., Bowen, J.E., Rosen, L.E., Saliba, C., Zepeda, S.K., Culap, K., Pinto, D., VanBlargan, L.A., De Marco, A., di Iulio, J., et al. (2022). Broadly neutralizing antibodies overcome SARS-CoV-2 Omicron antigenic shift. *Nature* 602, 664–670. <https://doi.org/10.1038/s41586-021-04386-2>.
- Cao, Y., Wang, J., Jian, F., Xiao, T., Song, W., Yisimayi, A., Huang, W., Li, Q., Wang, P., An, R., et al. (2022a). Omicron escapes the majority of existing SARS-CoV-2 neutralizing antibodies. *Nature* 602, 657–663. <https://doi.org/10.1038/s41586-021-04385-3>.
- Cao, Y., Yisimayi, A., Jian, F., Song, W., Xiao, T., Wang, L., Du, S., Wang, J., Li, Q., Chen, X., et al. (2022b). BA.2.12.1, BA.4 and BA.5 escape antibodies elicited by Omicron infection. *Nature* 608, 593–602. <https://doi.org/10.1038/s41586-022-04980-y>.
- Cathcart, L.A., Havenar-Daughton, C., Lempp, F.A., Ma, D., Schmid, M.A., Agostini, M.L., Guarino, B., Di Iulio, J., Rosen, L.E., Tucker, H., et al. (2021). The dual function monoclonal antibodies VIR-7831 and VIR-7832 demonstrate potent in vitro and in vivo activity against SARS-CoV-2. Preprint at bioRxiv. <https://doi.org/10.1101/2021.03.09.434607>.
- Cele, S., Jackson, L., Khoury, D.S., Khan, K., Moyo-Gwete, T., Tegally, H., San, J.E., Cromer, D., Scheepers, C., Amoako, D.G., et al. (2022). Omicron extensively but incompletely escapes Pfizer BNT162b2 neutralization. *Nature* 602, 654–656. <https://doi.org/10.1038/s41586-021-04387-1>.
- Chen, Z., Chumakov, K., Dragunsky, E., Kouliavskaja, D., Makiya, M., Neverov, A., Rezapkin, G., Sebrell, A., and Purcell, R. (2011). Chimpanzee-human monoclonal antibodies for treatment of chronic poliovirus excretors and emergency postexposure prophylaxis. *J. Virol.* 85, 4354–4362. <https://doi.org/10.1128/JVI.02553-10>.
- Chen, Z., Diaz, G., Pollicino, T., Zhao, H., Engle, R.E., Schuck, P., Shen, C.H., Zamboni, F., Long, Z., Kabat, J., et al. (2018). Role of humoral immunity against hepatitis B virus core antigen in the pathogenesis of acute liver failure. *Proc. Natl. Acad. Sci. USA* 115, E11369–E11378. <https://doi.org/10.1073/pnas.1809028115>.
- Chen, Z., Moayeri, M., Zhou, Y.H., Leppla, S., Emerson, S., Sebrell, A., Yu, F., Svitel, J., Schuck, P., St Claire, M., and Purcell, R. (2006). Efficient neutralization of anthrax toxin by chimpanzee monoclonal antibodies against protective antigen. *J. Infect. Dis.* 193, 625–633. <https://doi.org/10.1086/500148>.
- Corbett, K.S., Edwards, D.K., Leist, S.R., Abiona, O.M., Boyoglu-Barnum, S., Gillespie, R.A., Himansu, S., Schäfer, A., Ziwawo, C.T., DiPiazza, A.T., et al. (2020a). SARS-CoV-2 mRNA vaccine design enabled by prototype pathogen preparedness. *Nature* 586, 567–571. <https://doi.org/10.1038/s41586-020-2622-0>.
- Corbett, K.S., Flynn, B., Foulds, K.E., Francica, J.R., Boyoglu-Barnum, S., Werner, A.P., Flach, B., O’Connell, S., Bock, K.W., Minai, M., et al. (2020b). Evaluation of the mRNA-1273 vaccine against SARS-CoV-2 in nonhuman primates. *N. Engl. J. Med.* 383, 1544–1555. <https://doi.org/10.1056/NEJMoa2024671>.
- Corti, D., Purcell, L.A., Snell, G., and Veessler, D. (2021). Tackling COVID-19 with neutralizing monoclonal antibodies. *Cell* 184, 3086–3108. <https://doi.org/10.1016/j.cell.2021.05.005>.
- Davies, N.G., Abbott, S., Barnard, R.C., Jarvis, C.I., Kucharski, A.J., Munday, J.D., Pearson, C.A.B., Russell, T.W., Tully, D.C., Washburne, A.D., et al. (2021). Estimated transmissibility and impact of SARS-CoV-2 lineage B.1.1.7 in England. *Science* 372. <https://doi.org/10.1126/science.abg3055>.
- Davis, I.W., Murray, L.W., Richardson, J.S., and Richardson, D.C. (2004). MOLPROBITY: structure validation and all-atom contact analysis for nucleic acids and their complexes. *Nucleic Acids Res.* 32, W615–W619. <https://doi.org/10.1093/nar/gkh398>.
- De Giorgi, V., West, K.A., Henning, A.N., Chen, L.N., Holbrook, M.R., Gross, R., Liang, J., Postnikova, E., Trenbeath, J., Pogue, S., et al. (2021). Naturally acquired SARS-CoV-2 immunity persists for up to 11 Months following infection. *J. Infect. Dis.* 224, 1294–1304. <https://doi.org/10.1093/infdis/jiab295>.
- Dejnirattisai, W., Huo, J., Zhou, D., Zahradnik, J., Supasa, P., Liu, C., Duyvesteyn, H.M.E., Ginn, H.M., Mentzer, A.J., Tuekprakhon, A., et al. (2021). Omicron-B.1.1.529 Leads to Widespread Escape from Neutralizing Antibody Responses. <https://doi.org/10.1101/2021.12.03.471045>.
- Dejnirattisai, W., Huo, J., Zhou, D., Zahradnik, J., Supasa, P., Liu, C., Duyvesteyn, H.M.E., Ginn, H.M., Mentzer, A.J., Tuekprakhon, A., et al. (2022). SARS-CoV-2 Omicron-B.1.1.529 leads to widespread escape from neutralizing antibody responses. *Cell* 185, 467–484.e15. <https://doi.org/10.1016/j.cell.2021.12.046>.
- Doria-Rose, N.A., Shen, X., Schmidt, S.D., O’Dell, S., McDanal, C., Feng, W., Tong, J., Eaton, A., Magliano, M., Tang, H., et al. (2021). Booster of mRNA-1273 strengthens SARS-CoV-2 omicron neutralization. Preprint at medRxiv. <https://doi.org/10.1101/2021.12.15.21267805>.
- Du, L., Yang, Y., and Zhang, X. (2021). Neutralizing antibodies for the prevention and treatment of COVID-19. *Cell. Mol. Immunol.* 18, 2293–2306. <https://doi.org/10.1038/s41423-021-00752-2>.

- Elbe, S., and Buckland-Merrett, G. (2017). Data, disease and diplomacy: GISAID's innovative contribution to global health. *Global Chall.* *1*, 33–46. <https://doi.org/10.1002/gch2.1018>.
- Emsley, P., and Cowtan, K. (2004). Coot: model-building tools for molecular graphics. *Acta Crystallogr. D Biol. Crystallogr.* *60*, 2126–2132. <https://doi.org/10.1107/S0907444904019158>.
- Giudicelli, V., Chaume, D., and Lefranc, M.P. (2005). IMGT/GENE-DB: a comprehensive database for human and mouse immunoglobulin and T cell receptor genes. *Nucleic Acids Res.* *33*, D256–D261. <https://doi.org/10.1093/nar/gki010>.
- Glamann, J., Burton, D.R., Parren, P.W., Ditzel, H.J., Kent, K.A., Arnold, C., Montefiori, D., and Hirsch, V.M. (1998). Simian immunodeficiency virus (SIV) envelope-specific Fabs with high-level homologous neutralizing activity: recovery from a long-term-nonprogressor SIV-infected macaque. *J. Virol.* *72*, 585–592. <https://doi.org/10.1128/JVI.72.1.585-592.1998>.
- Greaney, A.J., Starr, T.N., Gilchuk, P., Zost, S.J., Binshtein, E., Loes, A.N., Hilton, S.K., Huddleston, J., Eguia, R., Crawford, K.H.D., et al. (2021). Complete mapping of mutations to the SARS-CoV-2 spike receptor-binding domain that escape antibody recognition. *Cell Host Microbe* *29*, 44–57.e9. <https://doi.org/10.1016/j.chom.2020.11.007>.
- Hammarström, L., Marcotte, H., Piralla, A., Baldanti, F., and Pan-Hammarström, Q. (2021). Antibody therapy for COVID-19. *Curr. Opin. Allergy Clin. Immunol.* *21*, 553–558. <https://doi.org/10.1097/ACI.0000000000000787>.
- Hachmann, N.P., Miller, J., Collier, A.R.Y., Ventura, J.D., Yu, J., Rowe, M., Bondzie, E.A., Powers, O., Surve, N., Hall, K., and Barouch, D.H. (2022). Neutralization escape by SARS-CoV-2 omicron subvariants BA.2.12.1, BA.4, and BA.5. *N. Engl. J. Med.* *387*, 86–88. <https://doi.org/10.1056/NEJMc2206576>.
- Hansen, J., Baum, A., Pascal, K.E., Russo, V., Giordano, S., Wloga, E., Fulton, B.O., Yan, Y., Koon, K., Patel, K., et al. (2020). Studies in humanized mice and convalescent humans yield a SARS-CoV-2 antibody cocktail. *Science* *369*, 1010–1014. <https://doi.org/10.1126/science.abd0827>.
- Hastie, K.M., Li, H., Bedinger, D., Schendel, S.L., Dennison, S.M., Li, K., Rayaprolu, V., Yu, X., Mann, C., Zandonatti, M., et al. (2021). Defining variant-resistant epitopes targeted by SARS-CoV-2 antibodies: a global consortium study. *Science* *374*, 472–478. <https://doi.org/10.1126/science.abh2315>.
- Henderson, R., Sali, A., Baker, M.L., Carragher, B., Devkota, B., Downing, K.H., Egelman, E.H., Feng, Z., Frank, J., Grigorieff, N., et al. (2012). Outcome of the first electron microscopy validation task force meeting. *Structure* *20*, 205–214. <https://doi.org/10.1016/j.str.2011.12.014>.
- Hsieh, C.L., Goldsmith, J.A., Schaub, J.M., DiVenere, A.M., Kuo, H.C., Javanmardi, K., Le, K.C., Wrapp, D., Lee, A.G., Liu, Y., et al. (2020). Structure-based design of prefusion-stabilized SARS-CoV-2 spikes. *Science* *369*, 1501–1505. <https://doi.org/10.1126/science.abd0826>.
- Iketani, S., Liu, L., Guo, Y., Liu, L., Chan, J.F.W., Huang, Y., Wang, M., Luo, Y., Yu, J., Chu, H., et al. (2022). Antibody evasion properties of SARS-CoV-2 Omicron sublineages. *Nature* *604*, 553–556. <https://doi.org/10.1038/s41586-022-04594-4>.
- Imai, M., Iwatsuki-Horimoto, K., Hatta, M., Loeber, S., Halfmann, P.J., Nakajima, N., Watanabe, T., Ujje, M., Takahashi, K., Ito, M., et al. (2020). Syrian hamsters as a small animal model for SARS-CoV-2 infection and countermeasure development. *Proc. Natl. Acad. Sci. USA* *117*, 16587–16595. <https://doi.org/10.1073/pnas.2009799117>.
- Jain, T., Sun, T., Durand, S., Hall, A., Houston, N.R., Nett, J.H., Sharkey, B., Bobrowicz, B., Caffry, I., Yu, Y., et al. (2017). Biophysical properties of the clinical-stage antibody landscape. *Proc. Natl. Acad. Sci. USA* *114*, 944–949. <https://doi.org/10.1073/pnas.1616408114>.
- Jones, B.E., Brown-Augsburger, P.L., Corbett, K.S., Westendorf, K., Davies, J., Cujec, T.P., Wiethoff, C.M., Blackbourne, J.L., Heinz, B.A., Foster, D., et al. (2021). The neutralizing antibody, LY-CoV555, protects against SARS-CoV-2 infection in nonhuman primates. *Sci. Transl. Med.* *13*, eabf1906. <https://doi.org/10.1126/scitranslmed.abf1906>.
- Kang, A.S., Barbas, C.F., Janda, K.D., Benkovic, S.J., and Lerner, R.A. (1991). Linkage of recognition and replication functions by assembling combinatorial antibody Fab libraries along phage surfaces. *Proc. Natl. Acad. Sci. USA* *88*, 4363–4366. <https://doi.org/10.1073/pnas.88.10.4363>.
- Kreye, J., Reincke, S.M., Kornau, H.C., Sánchez-Sendin, E., Corman, V.M., Liu, H., Yuan, M., Wu, N.C., Zhu, X., Lee, C.C.D., et al. (2020). A therapeutic non-self-reactive SARS-CoV-2 antibody protects from lung pathology in a COVID-19 hamster model. *Cell* *183*, 1058–1069.e19. <https://doi.org/10.1016/j.cell.2020.09.049>.
- Kucukelbir, A., Sigworth, F.J., and Tagare, H.D. (2014). Quantifying the local resolution of cryo-EM density maps. *Nat. Methods* *11*, 63–65. <https://doi.org/10.1038/nmeth.2727>.
- Liebschner, D., Afonine, P.V., Baker, M.L., Bunkóczi, G., Chen, V.B., Croll, T.I., Hintze, B., Hung, L.W., Jain, S., McCoy, A.J., et al. (2019). Macromolecular structure determination using X-rays, neutrons and electrons: recent developments in Phenix. *Acta Crystallogr. D Struct. Biol.* *75*, 861–877. <https://doi.org/10.1107/S2059798319011471>.
- Liu, L., Wang, P., Nair, M.S., Yu, J., Rapp, M., Wang, Q., Luo, Y., Chan, J.F.W., Sahi, V., Figueroa, A., et al. (2020). Potent neutralizing antibodies against multiple epitopes on SARS-CoV-2 spike. *Nature* *584*, 450–456. <https://doi.org/10.1038/s41586-020-2571-7>.
- Liu, X., Luongo, C., Matsuoka, Y., Park, H.S., Santos, C., Yang, L., Moore, I.N., Afroz, S., Johnson, R.F., Lafont, B.A.P., et al. (2021). A single intranasal dose of a live-attenuated parainfluenza virus-vectored SARS-CoV-2 vaccine is protective in hamsters. *Proc. Natl. Acad. Sci. USA* *118*, e2109744118. <https://doi.org/10.1073/pnas.2109744118>.
- Lusvardhi, S., Ayres, F., Hermanus, T., Madzivhandila, M., Kgagudi, P., Oos-thuysen, B., Lambson, B.E., de Oliveira, T., Vermeulen, M., van der Berg, K., et al. (2021). SARS-CoV-2 Omicron neutralization by therapeutic antibodies, convalescent sera, and post-mRNA vaccine booster. Preprint at bioRxiv. <https://doi.org/10.1101/2021.12.22.473880>.
- Mannar, D., Saville, J.W., Zhu, X., Srivastava, S.S., Berezuk, A.M., Tuttle, K.S., Marquez, A.C., Sekirov, I., and Subramaniam, S. (2022). SARS-CoV-2 Omicron variant: antibody evasion and cryo-EM structure of spike protein-ACE2 complex. *Science* *375*, 760–764. <https://doi.org/10.1126/science.abn7760>.
- Miguez-Rey, E., Choi, D., Kim, S., Yoon, S., and Săndulescu, O. (2022). Monoclonal antibody therapies in the management of SARS-CoV-2 infection. *Expert Opin. Invest. Drugs* *31*, 41–58. <https://doi.org/10.1080/13543784.2022.2030310>.
- Petersen, E.F., Goddard, T.D., Huang, C.C., Couch, G.S., Greenblatt, D.M., Meng, E.C., and Ferrin, T.E. (2004). UCSF Chimera—a visualization system for exploratory research and analysis. *J. Comput. Chem.* *25*, 1605–1612. <https://doi.org/10.1002/jcc.20084>.
- Piccoli, L., Park, Y.J., Tortorici, M.A., Czudnochowski, N., Walls, A.C., Beltramello, M., Silacci-Fregni, C., Pinto, D., Rosen, L.E., Bowen, J.E., et al. (2020). Mapping neutralizing and immunodominant sites on the SARS-CoV-2 spike receptor-binding domain by structure-guided high-resolution serology. *Cell* *183*, 1024–1042.e21. <https://doi.org/10.1016/j.cell.2020.09.037>.
- Planas, D., Saunders, N., Maes, P., Guivel-Benhassine, F., Planchais, C., Buchrieser, J., Bolland, W.H., Porrot, F., Staropoli, I., Lemoine, F., et al. (2022). Considerable escape of SARS-CoV-2 Omicron to antibody neutralization. *Nature* *602*, 671–675. <https://doi.org/10.1038/s41586-021-04389-z>.
- Prabakaran, P., Chen, W., Singarayan, M.G., Stewart, C.C., Streaker, E., Feng, Y., and Dimitrov, D.S. (2012). Expressed antibody repertoires in human cord blood cells: 454 sequencing and IMGT/HighV-QUEST analysis of germline gene usage, junctional diversity, and somatic mutations. *Immunogenetics* *64*, 337–350. <https://doi.org/10.1007/s00251-011-0595-8>.
- Qu, P., Faraone, J., Evans, J.P., Zou, X., Zheng, Y.M., Carlin, C., Bednash, J.S., Lozanski, G., Mallampalli, R.K., Saif, L.J., et al. (2022). Neutralization of the SARS-CoV-2 omicron BA.4/5 and BA.2.12.1 subvariants. *N. Engl. J. Med.* *386*, 2526–2528. <https://doi.org/10.1056/nejmc2206725>.
- Reed, L.J., and Muench, H. (1938). A simple method of estimating fifty per cent endpoints. *Am. J. Epidemiol.* *27*, 493–497.



- Rohou, A., and Grigorieff, N. (2015). CTFIND4: fast and accurate defocus estimation from electron micrographs. *J. Struct. Biol.* 192, 216–221. <https://doi.org/10.1016/j.jsb.2015.08.008>.
- Scheres, S.H.W. (2012). RELION: implementation of a Bayesian approach to cryo-EM structure determination. *J. Struct. Biol.* 180, 519–530. <https://doi.org/10.1016/j.jsb.2012.09.006>.
- Shang, J., Ye, G., Shi, K., Wan, Y., Luo, C., Aihara, H., Geng, Q., Auerbach, A., and Li, F. (2020). Structural basis of receptor recognition by SARS-CoV-2. *Nature* 581, 221–224. <https://doi.org/10.1038/s41586-020-2179-y>.
- Shi, R., Shan, C., Duan, X., Chen, Z., Liu, P., Song, J., Song, T., Bi, X., Han, C., Wu, L., et al. (2020). A human neutralizing antibody targets the receptor-binding site of SARS-CoV-2. *Nature* 584, 120–124. <https://doi.org/10.1038/s41586-020-2381-y>.
- Shrestha, L.B., Foster, C., Rawlinson, W., Tedla, N., and Bull, R.A. (2022). Evolution of the SARS-CoV-2 omicron variants BA.1 to BA.5: implications for immune escape and transmission. *Rev. Med. Virol.* 32, e2381. <https://doi.org/10.1002/rmv.2381>.
- Starr, T.N., Czudnochowski, N., Liu, Z., Zatta, F., Park, Y.J., Addetia, A., Pinto, D., Beltramello, M., Hernandez, P., Greaney, A.J., et al. (2021). SARS-CoV-2 RBD antibodies that maximize breadth and resistance to escape. *Nature* 597, 97–102. <https://doi.org/10.1038/s41586-021-03807-6>.
- Subbarao, K., McAuliffe, J., Vogel, L., Fahle, G., Fischer, S., Tatti, K., Packard, M., Shieh, W.J., Zaki, S., and Murphy, B. (2004). Prior infection and passive transfer of neutralizing antibody prevent replication of severe acute respiratory syndrome coronavirus in the respiratory tract of mice. *J. Virol.* 78, 3572–3577. <https://doi.org/10.1128/jvi.78.7.3572-3577.2004>.
- Takashita, E., Kinoshita, N., Yamayoshi, S., Sakai-Tagawa, Y., Fujisaki, S., Ito, M., Iwatsuki-Horimoto, K., Chiba, S., Halfmann, P., Nagai, H., et al. (2022). Efficacy of antibodies and antiviral drugs against covid-19 omicron variant. *N. Engl. J. Med.* 386, 995–998. <https://doi.org/10.1056/NEJMc2119407>.
- Tegally, H., et al. (2022). Emergence of SARS-CoV-2 Omicron lineages BA.4 and BA.5 in South Africa. *Nature Medicine* 28, 1785–1790. <https://doi.org/10.1038/s41591-022-01911-2>.
- Telenti, A., Arvin, A., Corey, L., Corti, D., Diamond, M.S., García-Sastre, A., Garry, R.F., Holmes, E.C., Pang, P.S., and Virgin, H.W. (2021). After the pandemic: perspectives on the future trajectory of COVID-19. *Nature* 596, 495–504. <https://doi.org/10.1038/s41586-021-03792-w>.
- Wang, P., Nair, M.S., Liu, L., Iketani, S., Luo, Y., Guo, Y., Wang, M., Yu, J., Zhang, B., Kwong, P.D., et al. (2021). Antibody resistance of SARS-CoV-2 variants B.1.351 and B.1.1.7. *Nature* 593, 130–135. <https://doi.org/10.1038/s41586-021-03398-2>.
- Waterhouse, A., Bertoni, M., Bienert, S., Studer, G., Tauriello, G., Gumienny, R., Heer, F.T., de Beer, T.A.P., Rempfer, C., Bordoli, L., et al. (2018). SWISS-MODEL: homology modelling of protein structures and complexes. *Nucleic Acids Res.* 46, W296–W303. <https://doi.org/10.1093/nar/gky427>.
- Westendorf, K., Žentelis, S., Wang, L., Foster, D., Vaillancourt, P., Wiggin, M., Lovett, E., van der Lee, R., Hendle, J., Pustilnik, A., et al. (2022). LY-CoV1404 (bebtelovimab) potently neutralizes SARS-CoV-2 variants. Preprint at bioRxiv. <https://doi.org/10.1101/2021.04.30.442182>.
- Wibmer, C.K., Ayres, F., Hermanus, T., Madzivhandila, M., Kgagudi, P., Oos-thuysen, B., Lambson, B.E., de Oliveira, T., Vermeulen, M., van der Berg, K., et al. (2021). SARS-CoV-2 501Y.V2 escapes neutralization by South African COVID-19 donor plasma. *Nat. Med.* 27, 622–625. <https://doi.org/10.1038/s41591-021-01285-x>.
- Wilhelm, A., Widera, M., Grikscheit, K., Toptan, T., Schenk, B., Pallas, C., Metzler, M., Kohmer, N., Hoehl, S., Helfritz, F.A., et al. (2021). Reduced neutralization of SARS-CoV-2 omicron variant by vaccine sera and monoclonal antibodies. Preprint at medRxiv. <https://doi.org/10.1101/2021.12.07.21267432>.
- Wrapp, D., Wang, N., Corbett, K.S., Goldsmith, J.A., Hsieh, C.L., Abiona, O., Graham, B.S., and McLellan, J.S. (2020). Cryo-EM structure of the 2019-nCoV spike in the prefusion conformation. *Science* 367, 1260–1263. <https://doi.org/10.1126/science.abb2507>.
- Yamasoba, D., Kimura, I., Nasser, H., Morioka, Y., Nao, N., Ito, J., Uriu, K., Tsuda, M., Zahradnik, J., Shirakawa, K., et al. (2022). Virological characteristics of SARS-CoV-2 BA.2 variant. Preprint at bioRxiv. <https://doi.org/10.1101/2022.02.14.480335>.
- Yewdell, J.W. (2021). Antigenic drift: understanding COVID-19. *Immunity* 54, 2681–2687. <https://doi.org/10.1016/j.immuni.2021.11.016>.
- Yu, J., Collier, A.Y., Rowe, M., Mardas, F., Ventura, J.D., Wan, H., Miller, J., Powers, O., Chung, B., Siamatu, M., et al. (2022). Comparable neutralization of the SARS-CoV-2 omicron BA.1 and BA.2 variants. Preprint at medRxiv. <https://doi.org/10.1101/2022.02.06.22270533>.
- Yuan, M., Liu, H., Wu, N.C., and Wilson, I.A. (2021). Recognition of the SARS-CoV-2 receptor binding domain by neutralizing antibodies. *Biochem. Biophys. Res. Commun.* 538, 192–203. <https://doi.org/10.1016/j.bbrc.2020.10.012>.
- Zhao, H., Boyd, L.F., and Schuck, P. (2017). Measuring protein interactions by optical biosensors. *Curr. Protoc. Protein Sci.* 88, 20.2.1–20.2.25. <https://doi.org/10.1002/cpps.31>.
- Zheng, S.Q., Palovcak, E., Armache, J.P., Verba, K.A., Cheng, Y., and Agard, D.A. (2017). MotionCor2: anisotropic correction of beam-induced motion for improved cryo-electron microscopy. *Nat. Methods* 14, 331–332. <https://doi.org/10.1038/nmeth.4193>.
- Zhou, H., Tada, T., Dcosta, B.M., and Landau, N.R. (2022). Neutralization of SARS-CoV-2 omicron BA.2 by therapeutic monoclonal antibodies. Preprint at bioRxiv. <https://doi.org/10.1101/2022.02.15.480166>.
- Zhou, P., Yang, X.L., Wang, X.G., Hu, B., Zhang, L., Zhang, W., Si, H.R., Zhu, Y., Li, B., Huang, C.L., et al. (2020). A pneumonia outbreak associated with a new coronavirus of probable bat origin. *Nature* 579, 270–273. <https://doi.org/10.1038/s41586-020-2012-7>.
- Zost, S.J., Gilchuk, P., Case, J.B., Binshtein, E., Chen, R.E., Nkolola, J.P., Schäfer, A., Reidy, J.X., Trivette, A., Nargi, R.S., et al. (2020a). Potently neutralizing and protective human antibodies against SARS-CoV-2. *Nature* 584, 443–449. <https://doi.org/10.1038/s41586-020-2548-6>.
- Zost, S.J., Gilchuk, P., Chen, R.E., Case, J.B., Reidy, J.X., Trivette, A., Nargi, R.S., Sutton, R.E., Suryadevara, N., Chen, E.C., et al. (2020b). Rapid isolation and profiling of a diverse panel of human monoclonal antibodies targeting the SARS-CoV-2 spike protein. *Nat. Med.* 26, 1422–1427. <https://doi.org/10.1038/s41591-020-0998-x>.

STAR★METHODS

KEY RESOURCES TABLE

REAGENT or RESOURCE	SOURCE	IDENTIFIER
<b>Antibodies</b>		
AffiniPure Goat Anti-Human IgG, Fc $\gamma$ fragment specific	Jackson ImmunoResearch	109-005-008
Peroxidase AffiniPure Goat Anti-Human IgG, Fc $\gamma$ fragment specific	Jackson ImmunoResearch	109-035-190
Peroxidase AffiniPure Goat Anti-Human IgG, F(ab') $_2$ fragment specific	Jackson ImmunoResearch	109-035-097
HRP/Anti-M13 Monoclonal Conjugate	Cytiva	27-9421-01
SARS-CoV-2 nucleoprotein-specific rabbit primary antibody	SinoBiological	40143-R001
Alexa 593-conjugated secondary antibody	Life technologies	A11037
1B1	This manuscript	N/A
3B6	This manuscript	N/A
2A12	This manuscript	N/A
1G8	This manuscript	N/A
3F6	This manuscript	N/A
4A12	This manuscript	N/A
4B6	This manuscript	N/A
4B7	This manuscript	N/A
4C6	This manuscript	N/A
A7	This manuscript	N/A
D12	This manuscript	N/A
G6	This manuscript	N/A
H11	This manuscript	N/A
NA8	This manuscript	N/A
NE8	This manuscript	N/A
NF8	This manuscript	N/A
NE12	This manuscript	N/A
NG3	This manuscript	N/A
REGN-10933	VRC, NIH	N/A
REGN-10987	VRC, NIH	N/A
LY-CoV555	VRC, NIH	N/A
LY-CoV016	VRC, NIH	N/A
S309	VRC, NIH	N/A
COV2-2196	VRC, NIH	N/A
COV2-2130	VRC, NIH	N/A
Anti-polio A12 IgG	<a href="#">Chen et al. (2011)</a>	N/A
<b>Bacterial and virus strains</b>		
SARS-CoV-2 wild-type	CDC	GenBank: MN985325
USA-WA-1/2020		GISAID: EPI_ISL_404895
SARS-CoV-2 lineage B.1.351/Beta	Johns Hopkins University	GISAID: EPI_ISL_890360
E. coli, TG1 strain	Lucigen	60502-1
M13KO7 helper phage	New England Biolabs	N0315S
E. coli, Top 10GF'	Lucigen	60061-2
5-alpha Competent E. coli	New England Biolabs	C2987H
Pseudovirus with SARS-CoV-2 S protein of Wuhan-1	This manuscript	GenBank: MN908947.3

(Continued on next page)

**Continued**

REAGENT or RESOURCE	SOURCE	IDENTIFIER
Pseudovirus with SARS-CoV-2 S protein of B.1.351	This manuscript	N/A
Pseudovirus with SARS-CoV-2 S protein of B.1.1.7	This manuscript	N/A
Pseudovirus with SARS-CoV-2 S protein of B.1.617.2	This manuscript	N/A
Pseudovirus with SARS-CoV-2 S protein of B.1.1.529	This manuscript	N/A
<b>Biological samples</b>		
Serum samples from convalescent COVID-19 patients	Blood bank of NIH	N/A
Whole blood samples from convalescent COVID-19 patients	Blood bank of NIH	N/A
<b>Chemicals, peptides, and recombinant proteins</b>		
SARS-CoV-2 (2019-nCoV) Spike RBD	SinoBiological	40592-V08H
Stabilized SARS-CoV-2 spike protein trimer (S-2P)	This manuscript	N/A
Stabilized SARS-CoV-2 spike protein trimer (S-6P)	This manuscript	N/A
Ficoll-Paque PLUS	Cytiva	17144002
293fectin transfection reagent	ThermoFisher Scientific	12347019
Turbo293 transfection reagent	Speed BioSystems	PXX1002
HisPur Ni-NTA resin	ThermoFisher Scientific	88221
Superdex 200 16/60	Cytiva	28-9893-35
Glucose	Sigma-Aldrich	G8270-5KG
PEG8000 (polyethylene glycol)	Sigma-Aldrich	89510-1KG-F
NaCl	Sigma-Aldrich	S9888-1KG
2xYT medium	IPM Scientific	11006-055
LB medium	IPM Scientific	11006-004
IPTG (isopropyl $\beta$ -D-thiogalactoside)	Sigma-Aldrich	I6758-10G
Ampicillin	ThermoFisher Scientific	J63807.09
Kanamycin sulfate	ThermoFisher Scientific	J17924_06
HiTrap SP HP	Cytiva	17115201
HiTrap Mab Select	Cytiva	28-4082-56
HisTrap HP	Cytiva	17-5248-02
Sensor chip CM5	Cytiva	BR-1000-2
ExpiFectamine 293 Transfection kit	ThermoFisher Scientific	A14524
Expi293 expression medium	ThermoFisher Scientific	A1435101
SureBlue™ TMB 1-Component Microwell Peroxidase Substrate	SeraCare	5120-0077
DMEM medium	ThermoFisher Scientific	11965092
Fetal bovine serum	Sigma-Aldrich	F4135
Penicillin-streptomycin	ThermoFisher Scientific	15140122
Puromycin	ThermoFisher Scientific	A1113803
Bright-Glo Luciferase assay substrate	Promega	E2620
XhoI	New England BioLabs	R0146M
SpeI-HF	New England BioLabs	R3133M
SacI-HF	New England BioLabs	R3156M
XbaI	New England BioLabs	R0145M
NheI-HF	New England BioLabs	R3131S
NotI	New England BioLabs	R3189S
Apal	New England BioLabs	R0114S
AgeI	New England BioLabs	R3552S

(Continued on next page)

<b>Continued</b>		
REAGENT or RESOURCE	SOURCE	IDENTIFIER
T4 DNA ligase	New England BioLabs	M0202M
Bovine Serum Albumine (BSA)	Sigma-Aldrich	3059
Tween 20	Sigma-Aldrich	93773
DMSO	Sigma-Aldrich	D2650
<b>Critical commercial assays</b>		
RNeasy mini kit	Qiagen	Cat#74106
First-strand cDNA synthesis kit	Cytiva	Cat#27926101
HotStarTaq DNA polymerase	Qiagen	Cat# 203205
<b>Deposited data</b>		
Antibody VH and VL sequences	This manuscript	GenBank: OM179962-OM179997
Ensemble cryo-EM map of the NE12/spike trimer complex	This manuscript	EMDB: EMD-26401
Local cryo-EM map of the NE12/spike trimer complex	This manuscript	EMDB: EMD-26402 Protein DataBank:7U9O
Ensemble cryo-EM maps of the NA8/spike trimer complex	This manuscript	EMDB: EMD-26403
Local cryo-EM maps of the NA8/spike trimer complex	This manuscript	EMDB: EMD-26404 Protein DataBank:7U9P
<b>Experimental models: Cell lines</b>		
Vero E6 cells	ATCC	CRL-1586
293 Freestyle cells	ThermoFisher Scientific	R79007
HEK293T/17 cells	ATCC	CRL-11268
ACE-2-expressing 293T cells (293T-hACE2.MF)	This manuscript	NA
Expi293F cells	ThermoFisher Scientific	A14527
<b>Experimental models: Organisms/strains</b>		
Golden Syrian hamster	Envigo Laboratories	N/A
<b>Oligonucleotides</b>		
Primers for PCR amplification of human $\gamma$ 1 heavy chain Fd	<a href="#">Glamann et al., (1998)</a>	N/A
Primers for PCR amplification of human $\kappa$ chain	<a href="#">Glamann et al., (1998)</a>	N/A
Primers for PCR amplification of human $\lambda$ chain	<a href="#">Kang et al. (1991)</a>	N/A
<b>Recombinant DNA</b>		
pComb3H	<a href="#">Barbas et al. (1991)</a>	N/A
IgG expression vector	This manuscript	N/A
<b>Software and algorithms</b>		
Prism version 9	GraphPad Software	N/A
Biacore T200 Evaluation software 3.1	Biaeval	N/A
EVILFIT	<a href="#">Zhao et al. (2017)</a>	N/A
CTFFind4	<a href="#">Rohou and Grigorieff, 2015</a>	N/A
MotionCorr2	<a href="#">Zheng et al., 2017</a>	N/A
RELION	<a href="#">Scheres, 2012</a>	N/A
UCSF Chimera	<a href="#">Pettersen et al., 2004</a>	N/A
ResMap	<a href="#">Kucukelbir et al., 2014</a>	N/A
Coot	<a href="#">Emsley and Cowtan, 2004</a>	N/A
Phenix	<a href="#">Liebschner et al., 2019</a>	N/A
<b>Other</b>		
Operetta high content imaging system	Perkin Elmer	N/A
Biacore T200	Cytiva	N/A
SpectraMax M5 plate reader	Molecular Devices	N/A
ÅKTA go	Cytiva	N/A

## RESOURCE AVAILABILITY

### Lead contact

Further information and requests for resources and reagents should be directed to and will be fulfilled by the Lead Contact, Patrizia Farci ([pfarci@niaid.nih.gov](mailto:pfarci@niaid.nih.gov)).

### Materials availability

Aliquots of antibodies will be made available by the [lead contact](#) upon request under a Material Transfer Agreement (MTA) for non-commercial usage.

### Data and code availability

- The antibody sequences reported in this paper have been deposited in the GenBank database (accession nos. OM179962-OM179997).
- The ensemble cryo-EM maps of the NE12/spike trimer and NA8/spike trimer complexes were deposited to the Electron Microscopy Data Bank (EMDB) with accession numbers EMD-26401 and EMD-26403, respectively. The locally refined maps of the NE12/spike trimer and NA8/spike trimer complexes were deposited to EMDB with accession numbers EMD-26402 and EMD-26404, respectively, and the corresponding coordinates were deposited to the Protein Data Bank with accession numbers 7U9O and 7U9P.
- Any additional information required to reanalyze the data reported is available from the [lead contact](#) upon request.

## EXPERIMENTAL MODEL AND SUBJECT DETAILS

### Convalescent COVID-19 plasma donor selection, human samples, and lymphocyte isolation

Convalescent COVID-19 plasma donors were prospectively enrolled onto an institutional review board-approved protocol (Clinical Trials Registration, NCT04360278) ([De Giorgi et al., 2021](#)) and provided written informed consent for the study. Among them, 12 convalescent plasma donors with high titer neutralizing antibodies against SARS-CoV-2 were selected, and 20-40 ml of blood was collected from each of them. Six of the 12 donors were females and 6 were males; their mean age was 54.6 years (range 35 to 66 years). Eligibility criteria included molecular or serologic evidence of past COVID-19 infection, and complete recovery from COVID-19, with no symptoms for  $\geq 28$  days or  $\geq 14$  days with a negative molecular test after recovery. PBMCs were prepared using density centrifugation on a Ficoll-Paque gradient.

## METHOD DETAILS

### Live virus neutralization assay used to test COVID-19 convalescent patients

Neutralization of live virus by patient plasmas was tested using a fluorescence reduction neutralization assay (FRNA) with SARS-CoV-2 [2019-nCoV/USA-WA1-A12/2020 (WA-1) from the US Centers for Disease Control and Prevention, Atlanta, GA, USA] at the NIH-NIAID Integrated Research Facility at Fort Detrick, MD, USA, as previously reported ([Bennett et al., 2021](#)). In these experiments, a fixed volume of diluted virus was incubated with an equivalent volume of test plasma for 1 hour at 37°C prior to adding the suspension to Vero E6 cells (ATCC, Manassas, VA, USA, #CRL-1586). The virus was allowed to propagate for 24 hours prior to fixing the cells. Following fixation, the cells were permeabilized and probed with a SARS-CoV-2 nucleoprotein-specific rabbit primary antibody (Sino Biological, Wayne, PA, USA, #40143-R001) followed by an Alexa594-conjugated secondary antibody (Life Technologies, San Diego, CA, USA, #A11037). The total number of infected cells in four fields per well with each field containing at least 1000 cells was quantified using an Operetta high content imaging system (Perkin Elmer, Waltham, MA, USA). Plasma was tested using two-fold serial dilutions from 1:40 to 1:1280 with four replicates per dilution. Results were calculated as the highest dilution of plasma leading to at least 50% reduction of SARS-CoV-2 titers. Each assay was controlled with internal addition of an S-specific neutralizing polyclonal antibodies. If a 1:40 dilution did not lead to at least 50% reduction of viral titer, results were reported as <1:40 even though some inhibition of virus propagation may have been present. To enable analysis of nAb kinetics over time, a value of 1:20 was used as a surrogate for results <1:40 since this value was the next serial 2-fold titer below the lowest positive result.

### Human Fab antibody library construction

Total RNA was extracted from PBMCs using RNeasy mini kit (Qiagen) and 1<sup>st</sup> strand cDNA was reverse transcribed with oligo(dT) as a primer with a kit from Cytiva and used as a template for antibody Fab coding fragment amplification. Briefly, the  $\gamma 1$  heavy chain Fd (variable and first constant region) was amplified with nine human heavy chain-specific 5' primers and a human  $\gamma 1$ -specific 3' primer. The  $\kappa$  chain was amplified by PCR with seven human  $\kappa$  chain-specific 5' primers and a 3' primer matching the end of the constant region ([Glamann et al., 1998](#)). The  $\lambda$  chain was amplified by PCR with six human  $\lambda$  chain-specific 5' primers and a 3' primer matching the end of the constant region ([Kang et al., 1991](#)). PCR was performed for 30 cycles at 95°C for 1 min, 52°C for 1 min, and 72°C for 1 min with HotStar Taq DNA polymerase (Qiagen). Amplified  $\kappa$  and  $\lambda$  chain DNA fragments were pooled, purified, digested with SacI

and XbaI. The restriction enzyme digested light chain fragments from one donor or pooled from 5 donors were then cloned into the pComb 3H vector by electroporation (Barbas et al., 1991). The recombinant plasmid DNA was introduced into *Escherichia coli* Top 10 cells (Lucigen) by electroporation, yielding  $1 \times 10^7$  individual clones. The plasmid DNA containing light chain sequences was digested with XhoI and SpeI, ligated with  $\gamma$ 1 Fd DNA cut with the same enzymes. The plasmid DNAs containing light and heavy chains were transformed into *E. coli* Top 10 cells by electroporation. Four phage display Fab libraries with average size of  $5 \times 10^8$  individual clones for each library were generated.

### Expression and purification of recombinant SARS-CoV-2 spike protein trimers

The stabilized SARS-CoV-2 spike protein trimer (S-2P) was produced by transient transfection of 293 Freestyle cells as previously described (Wrapp et al., 2020). One liter of 293 Freestyle cells at concentration of about 0.9 million cells per ml was transfected with 1 mg of S-2P plasmid, pre-mixed with 1 ml of 293fectin™ Transfection Reagent. The cells were allowed to grow for 6–7 days at 125 rpm, 37°C, and 8 % CO<sub>2</sub>; then the supernatant was harvested by centrifugation and filtered through Millipore Sigma 0.22  $\mu$ m PES filter. The cleared supernatant was incubated with 5 mL of HisPur™ Ni-NTA Resin ThermoFisher for three hours, then the resin was collected and washed with PBS with 25 mM imidazole, pH 7.4. The captured SARS-CoV-2 S-2P was eluted by PBS with 250 mM imidazole, pH 7.4. After elution, the trimeric protein was collected, concentrated, and applied to a Superdex 200 16/60 gel filtration column equilibrated with PBS. Peak fractions were pooled and concentrated to 1 mg/mL. The SARS-CoV-2 S-6P trimer was expressed and purified as previously described (Hsieh et al., 2020). Briefly, 1 mg of DNA encoding the S-6P spike was transfected into 293 Freestyle cells using Turbo293 transfection reagent (Speed BioSystems). The cells were grown at 37°C for 6 days, after which the supernatant was harvested and applied to His-Pure affinity resin. The resin was washed with 20 mM imidazole in PBS, and the protein eluted with 20 mM HEPES, pH 7.5, 200 mM NaCl and 300 mM imidazole. The trimeric protein was further purified on a Superdex S-200 gel filtration column equilibrated in PBS and concentrated to 1 mg/ml and flash frozen in liquid nitrogen for storage at –80°C.

### Selection of specific Fab clones

For phage production, 25 ml of logarithmic bacteria culture (OD<sub>600</sub> = 0.6) in 2×YT supplemented with 100  $\mu$ g/mL ampicillin and 2% glucose (2×YT-Amp-Glu) were infected with M13KO7 helper phage (New England Biolabs, USA) at  $7 \times 10^9$  plaque forming unit (PFU) per mL (~1:20 multiplicity of infection) by incubating at 37°C for 30 min without shaking, followed by 30 min at 120 rpm. Infected cells were harvested by centrifugation (5000 g for 5 min) and resuspended in 100 ml 2×YT supplemented with 100  $\mu$ g/mL ampicillin and 50  $\mu$ g/mL kanamycin. After overnight growth at 30°C at 250 rpm, the cells were removed by centrifugation (18000 g at 4°C for 20 min). The culture supernatant containing the phages was filtered through a 0.45- $\mu$ m filter and then precipitated with 1/5 volume of 20% PEG8000 (polyethylene glycol) in a 2.5 M NaCl solution, for 1 h on ice. Phage particles were pelleted by centrifugation (9000 g at 4°C for 20 min) and re-dissolved in 1 mL 1×PBS.

The phage library was panned by affinity binding of Fab-expressing phages on S-2P coated on the wells of an ELISA plate. Blocking of plates and phages was conducted for 60 min using 3% skimmed milk in 1×PBS. All washing steps were performed using PBS containing 0.05% Tween20 (PBST). For each panning cycle, 1  $\mu$ g/mL antigen was used to coat the polystyrene plate and after an overnight incubation, plates were washed and blocked. For the first panning cycle, approximately  $1 \times 10^{11}$  phages were incubated with the antigen coated plates for 2 h, followed by a total of 20 washes with PBST. The eluted phages were amplified in *E. coli* Top 10 cells. Bacterial culture was plated on 2×YT Amp-Glu agar and incubated overnight at 30°C. Clones were harvested into 5 ml 2×YT-Amp-Glu and phage production for the next round of panning, which was conducted in 40 ml medium, as described above. Two additional panning cycles were repeated using the same protocol. Following three cycles of panning, the selected phages were used for infection of *E. coli*. Single colonies were randomly picked from the third cycle output and screening of specific binders was performed, using phage ELISA against S-2P, with a BSA coated-plate as a negative control.

### Sequence analysis of S-2P-positive Fab clones

We sequenced the heavy-chain variable region (VH-DH-JH genes) of the ELISA-positive SARS-CoV-2 S-2P-specific clones obtained from each library using the Applied BioSystems model 3730 automated DNA sequencer with a modified Sanger method. The closest human germline V(D)J gene segments for each unique sequence were determined using DNAPLOT with IMGT sequence database (<http://www.imgt.org/IMGT>) (Giudicelli et al., 2005). The framework and CDRs were assigned according to IMGT nomenclature. The somatic mutations were identified by comparison of V-genes (from framework 1 to 3) with the closest germline counterpart. The first 28 nucleotides corresponding to the primer sequence were not included in the analysis. The distribution of VH and JH gene usage and HC-DR3 length of anti-SARS-CoV-2 was analyzed.

### Expression and purification of Fab and IgG

The phagemid containing light chain and heavy chain was cleaved with NheI and SpeI and re-circularized after removal of the phage gene III DNA fragment from the vector to encode soluble Fab. Bacteria containing circularized DNA without phage gene III were cultured in 2×TY medium containing 2% glucose, 100  $\mu$ g/mL ampicillin, and 15  $\mu$ g/mL tetracycline at 30°C until the OD<sub>600</sub> reached 0.5–1. The culture was diluted 5-fold in 2×YT medium without glucose and containing 0.2 mM isopropyl  $\beta$ -D-thiogalactoside (IPTG), and culture was continued at 27°C for 20 h for expression of soluble Fab. Because the Fab was tagged at the C terminus with (His)<sub>6</sub>,

the expressed proteins were affinity-purified on a nickel-charged column and were further purified through a cation-exchange SP column (Cytiva).

For IgG production, Expi293F™ cells (Thermo Fisher) were transiently transfected with plasmids carrying the antibody heavy chain and light chains. Cells were grown for six days at 37°C with 8% CO<sub>2</sub> shaking at 125 rpm according to the manufacturer's protocol (Thermo Fisher). Cell cultures were harvested six days after transfection and centrifuged at 20,000 g for 30 min at 4°C. The supernatants were collected and filtrated through a 0.22 μm filter. The expressed IgGs were purified by affinity chromatography on an immobilized protein G column (Cytiva). The purity of the Fab and IgG was evaluated by sodium dodecyl sulfate-polyacrylamide gel electrophoresis (SDS-PAGE), and the protein concentrations were determined by optical density (OD) measurements at 280 nm, with an A280 of 1.5 corresponding to 1.0 mg/mL.

### ELISA assays

For conventional antigen-binding ELISA, 96-well plates were coated with 100 μl/well containing 1 μg/mL protein in 1 × PBS (pH 7.4) and incubated at room temperature overnight. Serial dilutions of soluble Fab, IgG, or phage were added to the wells, and plates were incubated for 2 h at room temperature. The plates were washed, and the secondary conjugated antibody (anti-human Fab-HRP, anti-human IgG Fc-HRP, or anti-M13-HRP) was added and incubated for 1 h at room temperature. The plates were washed, and the color was developed by adding tetramethylbenzidine reagent (KPL; Gaithersburg, MD), and the development was stopped with H<sub>2</sub>SO<sub>4</sub> after 10 min. The plates were read at OD<sub>450</sub> in an ELISA plate reader. The data were plotted, and the dose-response curves were generated with Prism software (Graphpad Software, Inc., San Diego, CA).

For RBD-competition ELISA, 96-well plates were coated with 100 μl/well containing 1 μg/mL of recombinant S-2P trimer in 1 × PBS (pH 7.4), and the plates were incubated at room temperature overnight. Each Fab was 3-fold serially diluted from a starting concentration of 3 μg/mL in 3% milk/PBS or in 3% milk/PBS containing recombinant RBD protein (Sino Biological) at fixed concentration (5 μg/mL). Following incubation for 2 h at room temperature, the plate was washed, and a secondary anti-human Fab-HRP antibody (Jackson ImmunoResearch) was added for 1 h at room temperature. The plate was then washed, and the reaction was developed by adding tetramethylbenzidine substrate (KPL; Gaithersburg, MD). The reaction was stopped after 10 min by addition of sulfuric acid. The plates were read at OD<sub>450</sub> in an ELISA plate reader. The data were plotted, and dose-response curves with and without inhibition with RBD were generated using Prism software (Graphpad Software, Inc., San Diego, CA).

For antibody cross-competition ELISA, 96-well ELISA plates were coated with 100 μl/well containing 1 μg/mL of recombinant S-2P trimer in 1 × PBS (pH 7.4) and the plates were incubated at room temperature overnight. To test cross-competition among the mAbs, the IgG version of each mAb was incubated at 0.1 μg/mL with each of 11 Fabs at 1 μg/mL. An in house-produced anti-poliovirus IgG antibody was used as a negative control (Chen et al., 2011). Following incubation for 2 h at room temperature, the plates were washed, and a secondary anti-human IgG Fc-HRP antibody (Jackson ImmunoResearch) was added and incubated for 1 h at room temperature. The plates were then washed, and the reaction was developed by adding tetramethylbenzidine substrate (KPL; Gaithersburg, MD). The reaction was stopped after 10 min by addition of sulfuric acid. The plates were read at OD<sub>450</sub> in an ELISA plate reader. The average value from three wells was used to calculate the percent competition using the following formula:  $[1 - (\text{average OD from wells containing test IgG with Fab} - \text{average OD from control wells}) / (\text{average OD from wells containing test IgG without Fab} - \text{average OD from control wells})] \times 100\%$ .

### Surface plasmon resonance (SPR)

The SPR experiments were performed on a Biacore™ T200 (Cytiva) at 25°C in 10 mM HEPES pH 7.2, 150 mM NaCl, 3 mM EDTA, 0.05% Tween-20. The recombinant SARS-CoV-2 spike 2p (S-2P) protein was immobilized on a Series S-CM5 sensor chip (Cytiva) by amine coupling (NHS/EDC) to flow cells. A mock coupled surface was used for background subtraction. Binding and kinetics studies were performed multiple times for each Fab. Increasing amounts of each Fab were injected over the surface at a flow rate of 30 μl/min with an association time of 120 sec and dissociation time of 180 sec, followed by a regeneration with 100mM CAPS, pH 11.5 for 90 sec. Binding data were analyzed using Biacore™ T200 Evaluation Software 3.1 (Biaeval) with fits to the Langmuir binding equation for a 1:1 interaction model. In addition, data were analyzed by surface site affinity distribution analysis by EVILFIT (Zhao et al., 2017). Values obtained with the two methods were consistent.

### Pseudotype neutralization assay

The SARS-Cov-2 pseudovirus neutralization assays were performed as previously reported (Corbett et al., 2020b). Briefly, single-round luciferase-expressing pseudoviruses were generated by co-transfection of plasmids encoding the full-length SARS-CoV-2 S protein (Wuhan-1, GenBank accession number, MN908947.3; B.1.351/Beta; B.1.1.7/Alpha; B.1.617.2./Delta; Omicron BA.1 and BA.2 sublineages; luciferase (pHR' CMV Luc), a lentivirus backbone (pCMV ΔR8.2), and human transmembrane protease serine 2 (TMPRSS2) at a ratio of 1:20:20:0.3 into HEK293T/17 cells (ATCC) using the transfection reagent LiFect293™. The pseudoviruses were harvested after 72 hours. The supernatants were collected by centrifugation at 1500 rpm for 10 minutes, then filtered through a 0.45 μm filter, aliquoted and titrated before the neutralization assay. To test antibody-mediated neutralization, an 8-point, 5-fold dilution series was prepared for each antibody in culture medium (DMEM medium supplemented with 10% fetal bovine serum, 1% penicillin-streptomycin and 3 μg/mL puromycin). Each antibody dilution (50 μL) was mixed with 50 μL of diluted pseudovirus in 96-well plates and incubated for 30 min at 37°C. The mixture was then incubated with 10<sup>4</sup> ACE-2-expressing 293T cells (293T-hACE2.MF) in

a final volume of 200  $\mu\text{L}$ . Seventy-two hours later, the supernatant was carefully removed, the cells were lysed with Bright-Glo™ Luciferase Assay substrate (Promega), and the luciferase activity (relative light units, RLU) was measured. Percent neutralization was normalized considering uninfected cells as 100% neutralization and cells infected in the absence of antibodies as 0% neutralization.  $\text{IC}_{50}$  titers were determined using a log (agonist) vs. normalized response (variable slope) nonlinear function in Prism v8 (GraphPad).

### Live virus neutralization assay

SARS-CoV-2 neutralization using live virus was determined in the BSL3 laboratory using SARS-CoV-2 USA-WA1/2020 [WA-1; GenBank MN985325; GISAID: EPI\_ISL\_404895; obtained from Dr. Natalie Thornburg, Centers for Disease Control and Prevention (CDC)] and USA/MD-HP01542/2021 (lineage B.1.351/Beta variant; GISAID: EPI\_ISL\_890360; obtained from Dr. Andrew Pekosz, Johns Hopkins University). WA-1 was passaged twice on Vero E6 cells. The USA/MD-HP01542/2021 was passaged on TMPRSS2-expressing Vero E6 cells. The SARS-CoV-2 stocks were titrated in Vero E6 cells by determination of the 50% tissue culture infectious dose ( $\text{TCID}_{50}$ ) as previously described (Subbarao et al., 2004). The mAbs were serially diluted in Opti-MEM and mixed with an equal volume of SARS-CoV-2 (100  $\text{TCID}_{50}$ ) and then incubated at 37°C for 1 h. Mixtures were added to quadruplicate wells of Vero E6 cells in 96-well plates and incubated for four days. The 50% neutralizing dose ( $\text{ND}_{50}$ ) was defined as the highest dilution of serum that completely prevented cytopathic effect in 50% of the wells and was expressed as a  $\log_{10}$  reciprocal value (Liu et al., 2021). The dilution of antibodies that completely prevented cytopathic effect in 50% of the wells ( $\text{ND}_{50}$ ) was calculated by the Reed and Muench formula (Reed and Muench, 1938).

### Cryo-EM specimen preparation and data collection

SARS-CoV-2 S-6P spike at a concentration of 0.5 mg/mL in PBS was mixed with Fab NA8 or Fab NE12 using a Fab-to-RBD molar ratio of 1:1, and the complex was used for specimen preparation after a brief (5–10 min) incubation at 4°C. To prepare cryo-EM specimens, Quantifoil R 2/2 gold grids were glow-discharged using a PELCO easiGlow device (air pressure: 0.39 mBar, current: 20 mA, duration: 30 s) immediately before vitrification using an FEI Vitrobot Mark IV plunger. The Vitrobot chamber was kept at 4°C and 95% humidity, and the drop volume was 2.7  $\mu\text{L}$ . Datasets were collected at the National CryoEM Facility (NCEF), National Cancer Institute, using a Thermo Scientific Titan Krios G3 electron microscope equipped with a K3 direct electron detector and Gatan Quantum GIF energy filter (slit width: 20 eV) (Table S4).

### Single particle analysis of cryo-EM data

Single particle analysis was performed using the Frederick Research Computing Environment (FRCE) computing cluster. MotionCorr2 was used for patch-based movie frame alignment (Zheng et al., 2017). Contrast transfer function parameters were estimated with ctfind 4.1 (Rohou and Grigorieff, 2015). The following steps were performed using Relion 3.1.0 (Scheres, 2012), unless otherwise stated. Particle picking was performed using the template-free Laplacian-Gaussian filter-based approach. Particles were first extracted with 4x binning and subjected to 2D and 3D classification, with the low-pass filtered cryo-EM map of individual SARS-CoV-2 S-2P spike at pH 7.4 serving as the initial 3D model. Particles contributing to high-quality 3D classes were then re-extracted with 2x binning, and the above procedure was repeated. Finally, the best particles were re-extracted without binning, and the 3D map was iteratively improved with rounds of 3D auto-refinement, CTF refinement, and Bayesian polishing. For local refinement, a soft mask encompassing one RBD in the down position with the bound Fab and the neighboring NTD was created after segmenting the refined ensemble map in UCSF Chimera (Pettersen et al., 2004) and used for auto-refinement with limited angular search (-sigma\_ang = 5). Resolution was calculated using the gold-standard approach (Henderson et al., 2012) at the FSC curve threshold of 0.143. Local resolution was determined with ResMap 1.1.4 (Kucukelbir et al., 2014).

### Atomic model generation

An RBD from the cryo-EM structure of the S-2P spike at pH 4.0 (PDB ID 6xlu) was docked into the locally refined cryo-EM map, along with an NTD from the same structure and a homology model of the corresponding Fab prepared using the SWISS-MODEL server (Waterhouse et al., 2018). The atomic model was refined by alternating rounds of model building in Coot (Emsley and Cowtan, 2004) and real-space refinement in Phenix (Liebschner et al., 2019). Structure validation was performed with Molprobity (Davis et al., 2004). Map-model correlations were evaluated with phenix.mtriage (Afonine et al., 2018). Molecular graphics and analyses were performed with UCSF Chimera (Pettersen et al., 2004).

### Prophylactic and therapeutic studies in the hamster model

The hamster studies were approved by the NIAID Animal Care and Use Committee. All the animal experiments were carried out following the Guide for the Care and Use of Laboratory Animals by the NIH. Golden Syrian hamsters (*Mesocricetus auratus*, Envigo Laboratories, Frederick, MD) were used in experiments conducted in BSL2 and BSL3 facilities approved by the USDA and CDC. In the prophylactic study, 80 male Syrian hamsters, aged 8–9 weeks, were randomly divided into groups of 10 animals each, bled for baseline serology and inoculated intraperitoneally with 0.5 mL of NE12, NA8, or IgG1 control at 12 mg/kg or 4 mg/kg, diluted to the concentration of 2.4 mg/mL or 0.8 mg/mL in PBS. Twenty-four hours later, the animals were challenged intranasally with 4.5  $\log_{10}$   $\text{TCID}_{50}$  of SARS-CoV-2 WA-1 or B.1.351 in 100  $\mu\text{L}$  volumes of L-15 medium (ThermoFisher) per animal. Intranasal instillations



were performed under light isoflurane anesthesia. Animals were euthanized by CO<sub>2</sub> inhalation prior to necropsy. Body weights and clinical symptoms were monitored daily from day –3 before challenge through day 5 after challenge. On days 3 and 5 post-challenge, 5 animals per group were necropsied; nasal turbinate and lung tissues were collected. Tissues were weighed, mixed with L-15 medium (10 mL per gram of tissue), homogenized, and clarified by centrifugation. Aliquots were snap-frozen and stored at –80°C. The presence of the challenge virus in clarified tissue homogenates was evaluated by limiting-dilution titrations on Vero E6 cells. The titration of SARS-CoV-2 was performed by determination of the TCID<sub>50</sub> in Vero E6 cells and expressed as TCID<sub>50</sub> per gram of tissue, as previously described (Subbarao et al., 2004).

In the therapeutic study, 60 male Syrian hamsters, aged 9–10 weeks, were randomly divided into three groups of 10 animals each, bled for serology and inoculated intranasally with 4.5 log<sub>10</sub> TCID<sub>50</sub> of SARS-CoV-2 WA-1 or B.1.351 in 100 μL volumes per animal. Twenty-four hours later, the animals were inoculated intraperitoneally with 0.5 mL of NE12, NA8, or IgG1 control at 12 mg/kg, diluted to the concentration of 2.4 mg/mL in PBS. Body weights and clinical symptoms were monitored daily from day –4 before virus inoculation through day 11 after inoculation. On day 3 post-inoculation, five animals per group were necropsied; nasal turbinates and lungs were collected and processed as above. Virus titers were determined by limiting-dilution titrations on Vero E6 cells as described above (Subbarao et al., 2004).

## QUANTIFICATION AND STATISTICAL ANALYSIS

### Statistical analysis

Data sets were assessed for significance using one-way ANOVA with Tukey's multiple comparison test, or, if indicated, by non-parametric Kruskal-Wallis test with a Benjamini, Krieger and Yekutieli false-discovery test. Statistical comparisons of weight changes between treatment groups were performed using a repeated-measures mixed-effects model with Tukey's multiple-comparison test. Data were only considered significant at  $p < 0.05$ . Analyses were performed using Prism 9 (GraphPad Software).

**Supplemental information**

**Potent monoclonal antibodies neutralize**

**Omicron sublineages and other SARS-CoV-2 variants**

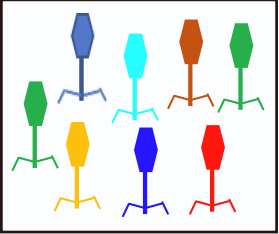
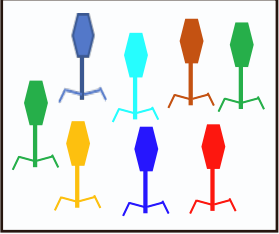
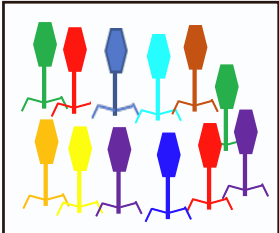
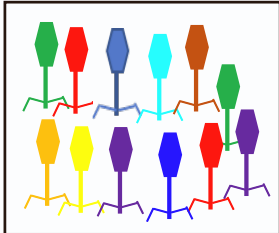
**Zhaochun Chen, Peng Zhang, Yumiko Matsuoka, Yaroslav Tsybovsky, Kamille West, Celia Santos, Lisa F. Boyd, Hanh Nguyen, Anna Pomerence, Tyler Stephens, Adam S. Olin, Baoshan Zhang, Valeria De Giorgi, Michael R. Holbrook, Robin Gross, Elena Postnikova, Nicole L. Garza, Reed F. Johnson, David H. Margulies, Peter D. Kwong, Harvey J. Alter, Ursula J. Buchholz, Paolo Lusso, and Patrizia Farci**

**Cell Reports**

**Supplemental Information**

**Potent monoclonal antibodies neutralize  
Omicron sublineages and other SARS-CoV-2 variants**

Zhaochun Chen, Peng Zhang, Yumiko Matsuoka, Yaroslav Tsybovsky, Kamille West,  
Celia Santos, Lisa F. Boyd, Hanh Nguyen, Anna Pomerence, Tyler Stephens,  
Adam S. Olia, Baoshan Zhang, Valeria De Giorgi, Michael R. Holbrook, Robin Gross,  
Elena Postnikova, Nicole L. Garza, Reed F. Johnson, David H. Margulies,  
Peter D. Kwong, Harvey J. Alter, Ursula J. Buchholz, Paolo Lusso, Patrizia Farci

<b>Single patient</b>		<b>Patient number</b>	<b>Neutralizing titer</b>	<b>Library size</b>	<b>Positive clones</b>	<b>Distinct clones</b>			
<b>Library 1</b>		1	80	$4.2 \times 10^7$	12	1			
									
<b>Library 2</b>		2	80	$4.0 \times 10^7$	70	3			
									
<b>Multiple patients</b>		<b>Patient number</b>	<b>Neutralizing titer</b>	<b>Library size</b>	<b>Positive clones</b>	<b>Distinct clones</b>			
<b>Library 3</b>		3	80	$9.1 \times 10^8$	300	9			
		4	80						
		5	320						
		6	320						
		7	320						
<b>Library 4</b>		8	160				$7.8 \times 10^8$	230	5
		9	160						
		10	640						
		11	160						
		12	640						

**Figure S1. Characteristics of 4 phage-display Fab libraries, related to Figure 1.** The libraries were generated from peripheral blood mononuclear cells (PBMC) obtained from convalescent COVID-19 donors, derived from either a single donor or five donors combined.

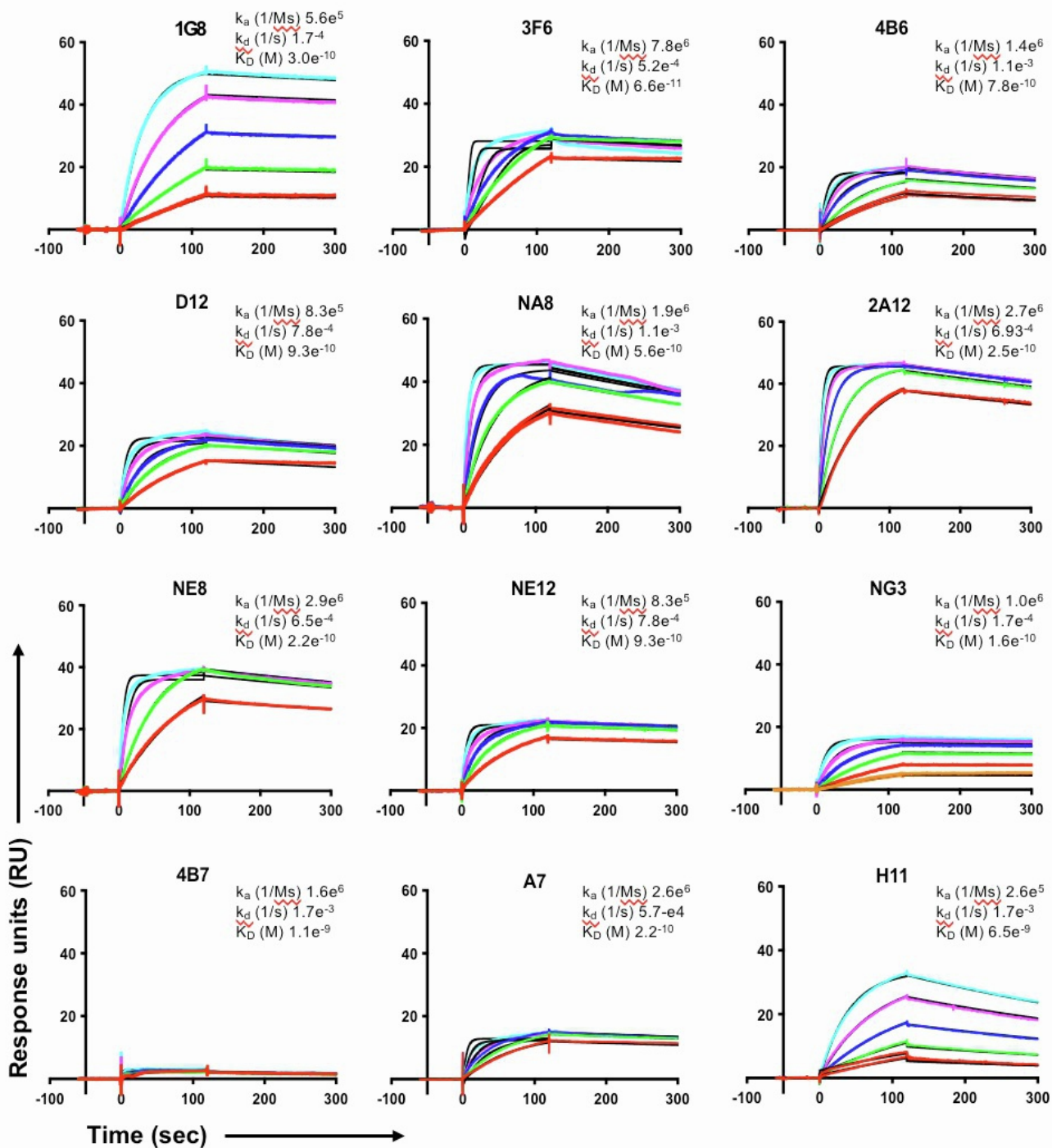


**Figure S2. Binding profiles of 12 Fabs to a stabilized trimeric SARS-CoV-2 spike protein (S-2P), related to Figure 1.** All the Fabs showed tight binding to the protein. The S-2P protein was coupled to the chip at a surface density 200-450 Rus. Fabs were flowed over the surface at graded concentrations ranging from 5.625 nM to 90 nM (color coded). Kinetic values were obtained using Biaeval 3.1; fits are indicated by the black lines.

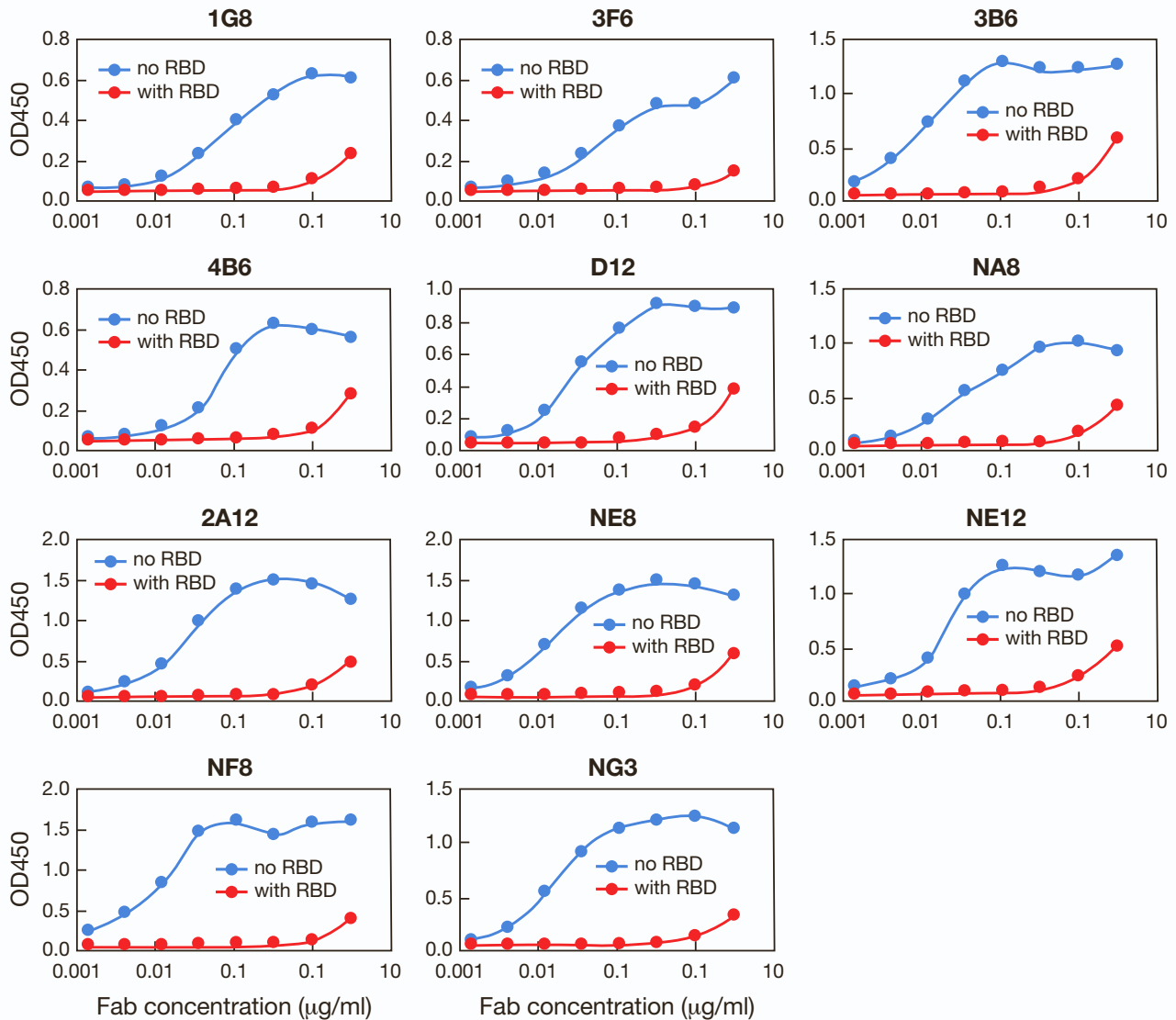


**Figure S3. Binding of 12 Fabs derived from convalescent COVID-19 donors to the receptor-binding domain (RBD) of the SARS-CoV-2 spike protein, related to Figure 2.** All of the Fabs shown, except one, are specific for the RBD, as demonstrated using the recombinant RBD protein as a competitor in ELISA. The red lines show the loss of signal when recombinant RBD was pre-incubated with the Fabs. Only one Fab, H11, was not inhibited, suggesting that its binding site is outside the RBD.

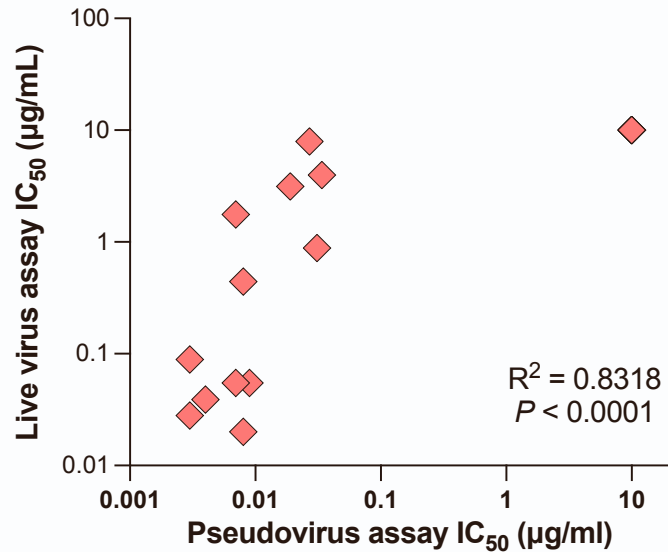
		Fab →										
		NE12	NF8	NG3	1G8	3B6	3F6	4B6	D12	NA8	NE8	2A12
IgG ↓	NE12	84	99	97	-31	90	30	58	58	62	85	82
	NF8	78	99	67	-17	94	16	75	97	85	98	86
	NG3	70	93	91	-64	93	57	98	84	72	82	75
	1G8	41	73	45	92	72	92	84	86	82	87	42
	3B6	55	87	61	-49	96	4	83	89	99	93	99
	3F6	27	33	24	64	16	86	27	34	47	22	18
	4B6	93	95	86	-38	98	5	80	87	81	97	78
	D12	81	93	83	-30	95	6	74	80	61	86	87
	NA8	69	88	65	-82	92	-18	37	63	51	74	76
	NE8	46	78	41	-60	78	-19	18	47	42	61	61
	2A12	68	88	70	-59	94	-15	28	66	64	84	86

**Figure S4. Cross-competition of 11 monoclonal antibodies for binding to the SARS-CoV-2 spike protein (S-2P) trimer, related to Figure 2.** To investigate if the epitopes recognized by the 11 monoclonal antibodies are distinct or overlapping, we performed cross-competition experiments between Fabs and complete IgG in ELISA. The percent competition was calculated using the following formula:  $[1 - (\text{average OD from wells containing test IgG with Fab} - \text{average OD from control wells}) / (\text{average OD from wells containing test IgG without Fab} - \text{average OD from control wells})] \times 100\%$ .

**A**

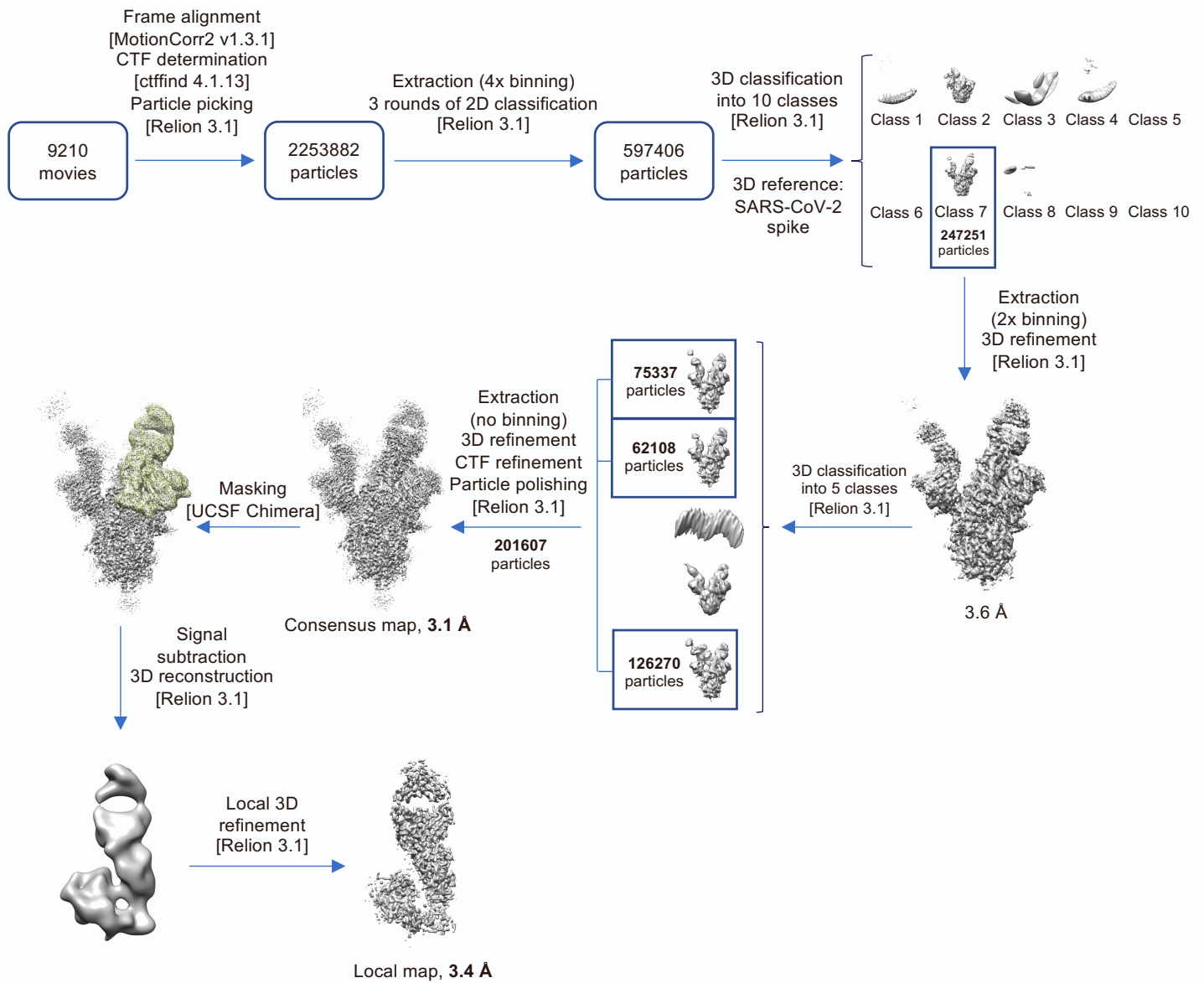
mAb	Live virus neutralization IC <sub>50</sub> (µg/ml)	
	WA-1	B.1.351 Beta
G6	>10	>10
4A12	>10	>10
4B7	>10	>10
A7	>10	>10
1B1	>10	>10
4C6	>10	>10
H11	>10	>10
1G8	3.969	0.298
3F6	3.150	0.221
3B6	0.020	>10
4B6	7.937	>10
D12	1.768	>10
NA8	0.442	0.039
2A12	0.039	>10
NE8	0.055	>10
NE12	0.028	>10
NF8	0.884	>10
NG3	0.055	>10
Lilly_CoV555	0.089	>10

>10	10-1	1-0.1	0.1-0.01	<0.01
-----	------	-------	----------	-------

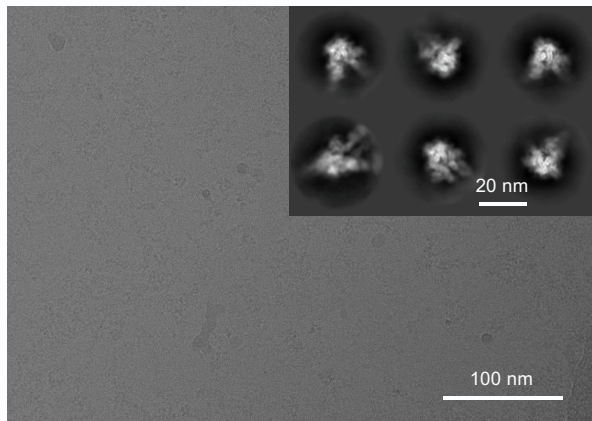
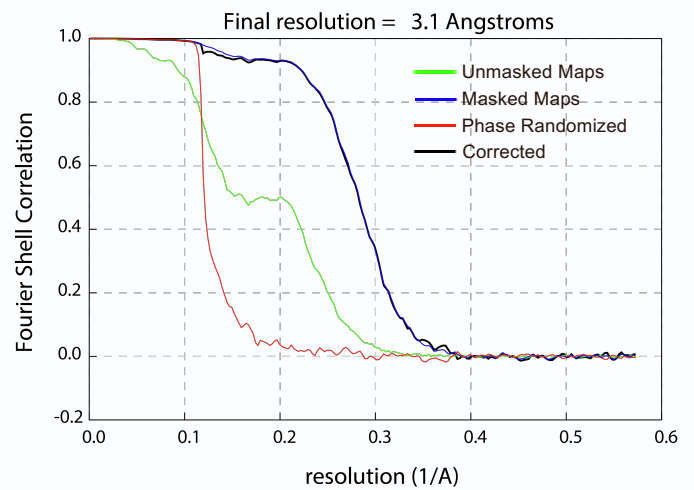
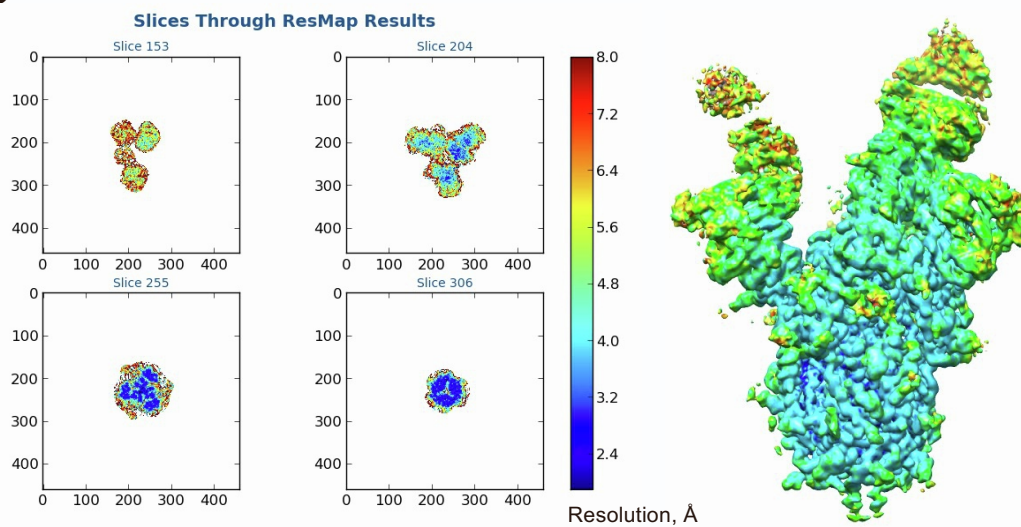
**B**

**Figure S5. Live virus neutralization of WA-1 and B.1.351 SARS-CoV-2 strains by 18 monoclonal antibodies and correlation with pseudovirus neutralization, related to Figure 2. (A) Heat map of live virus neutralization against SARS-CoV-2 WA-1 and B.1.351. (B) Correlation between neutralizing activities of mAbs in the pseudovirus and live virus assays.**





**Figure S6. Cryo-EM data processing workflow leading to the structure of SARS-CoV-2 Spike in complex with Fab NE12, related to Figure 3. Software packages are indicated in square brackets.**

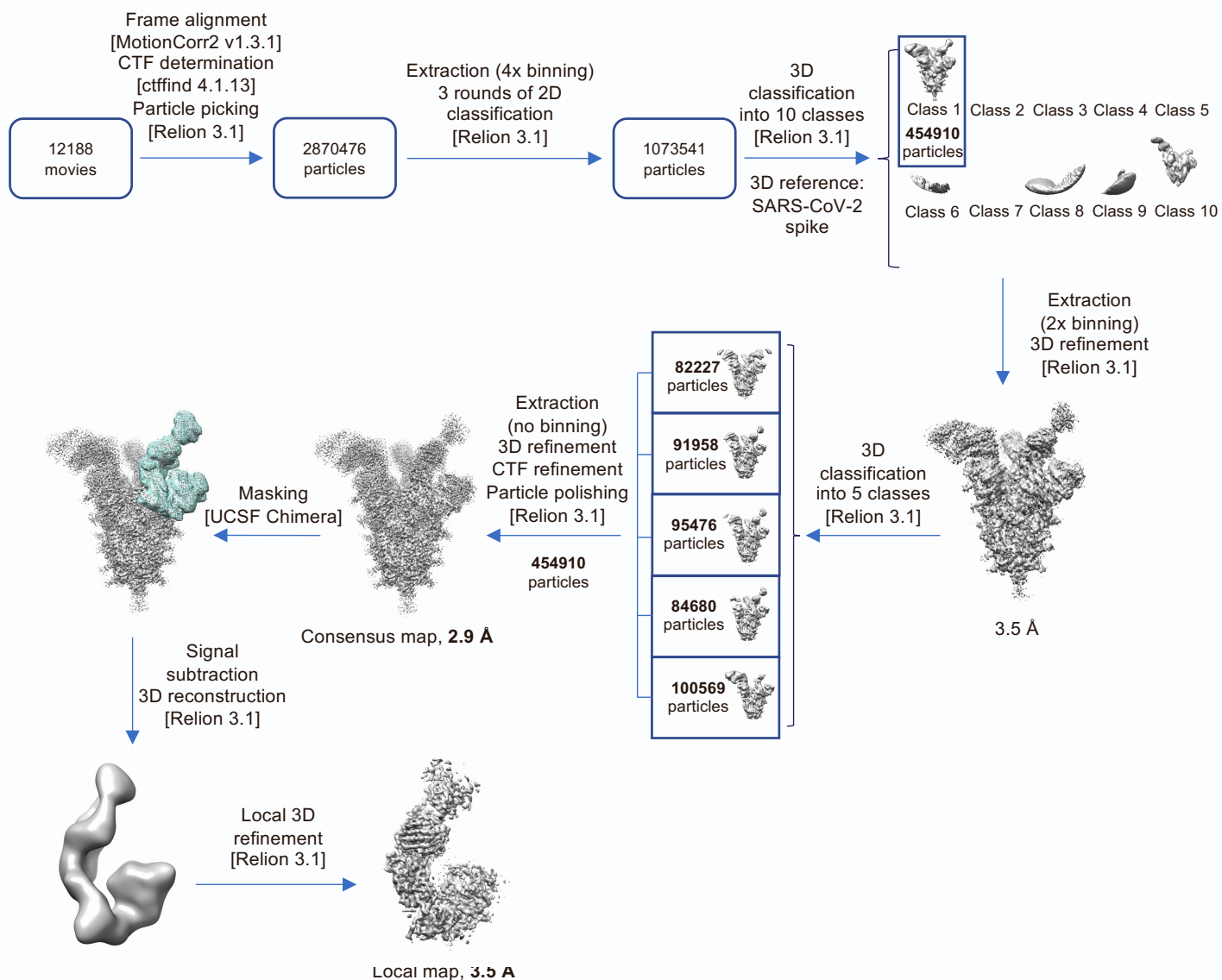
**A****B****C**

**Figure S7. Validation of the consensus cryo-EM map of SARS-CoV-2 spike in complex with Fab NE12, related to Figure 3.**

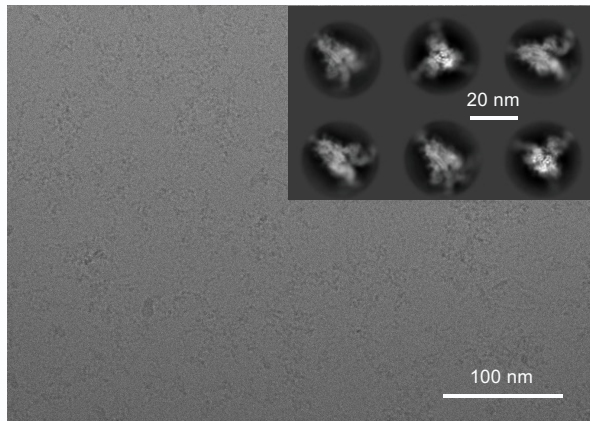
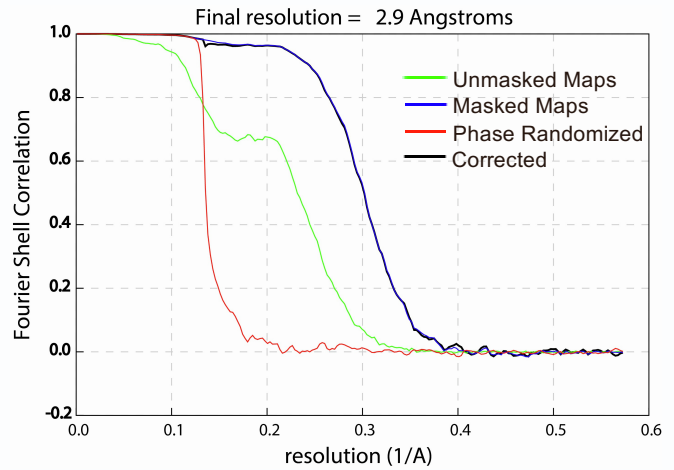
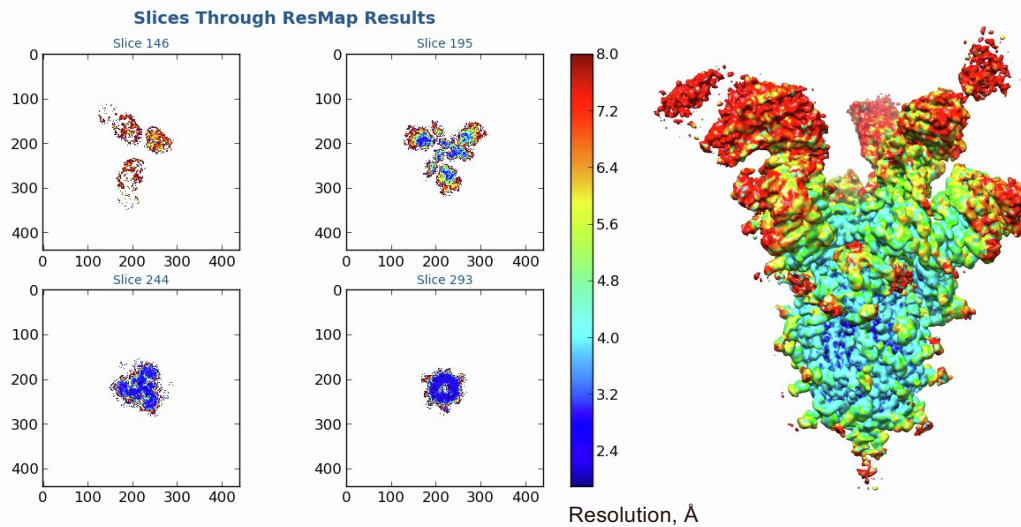
(A) Representative micrograph and 2D classes (insert).

(B) Fourier shell correlation (FSC) plots generated by Relion.

(C) Local resolution determined with ResMap.



**Figure S8. Cryo-EM data processing workflow leading to the structure of SARS-CoV-2 Spike in complex with Fab NA8, related to Figure 4. Software packages are indicated in square brackets.**

**A****B****C**

**Figure S9. Validation of the consensus cryo-EM map of SARS-CoV-2 spike in complex with Fab NA8, related to Figure 4.**

- (A) Representative micrograph and 2D classes (insert).  
 (B) Fourier shell correlation (FSC) plots generated by Relion.  
 (C) Local resolution determined with ResMap.

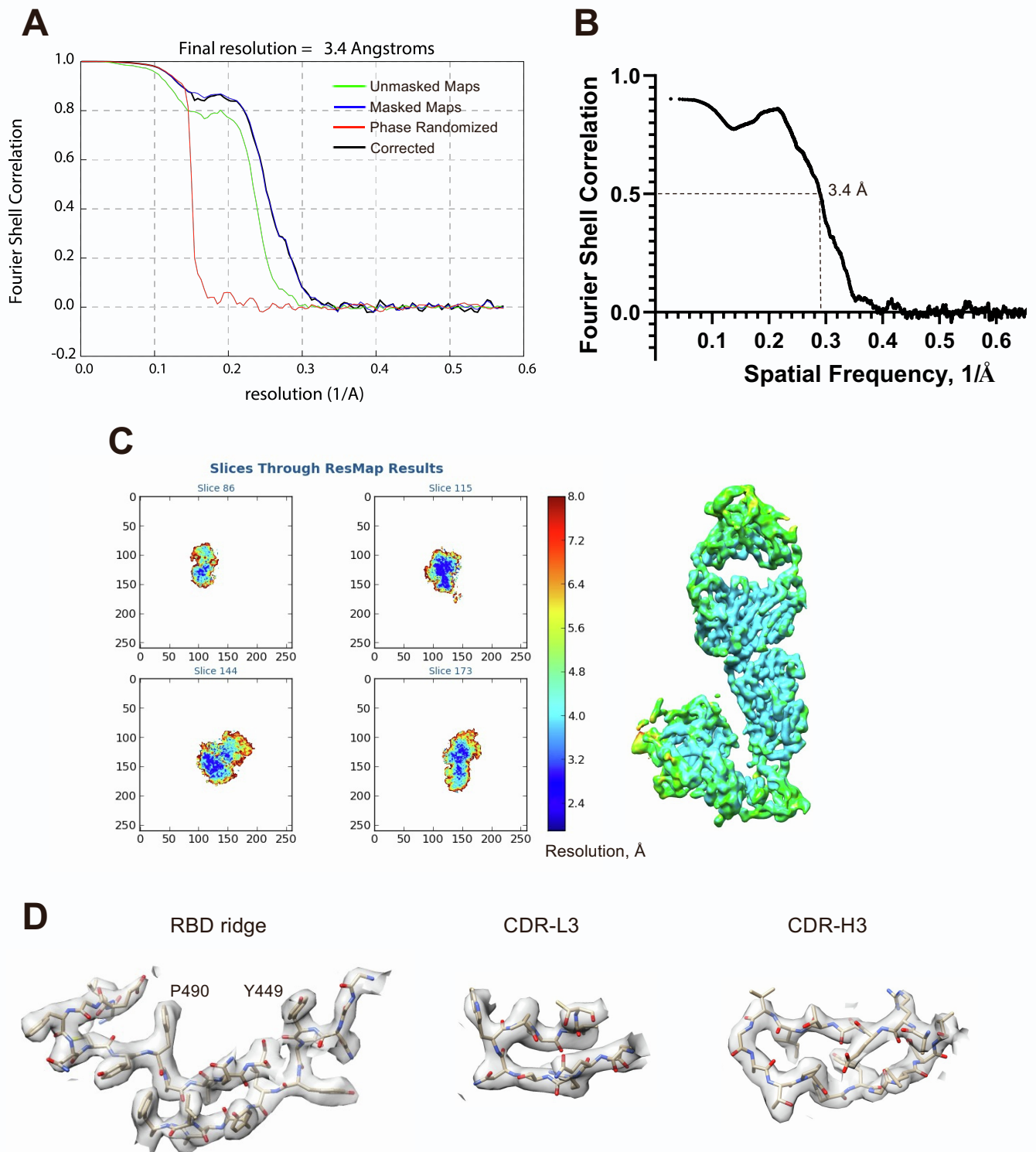


**Figure S10. Validation of the local cryo-EM structure of SARS-CoV-2 receptor binding domain (RBD) in complex with Fab NE12, related to Figure 3.**

(A) Fourier shell correlation (FSC) plots generated by Relion.

(B) FSC curve between the map and atomic model.

(C) Local resolution determined with ResMap.

(D) Examples of cryo-EM density.

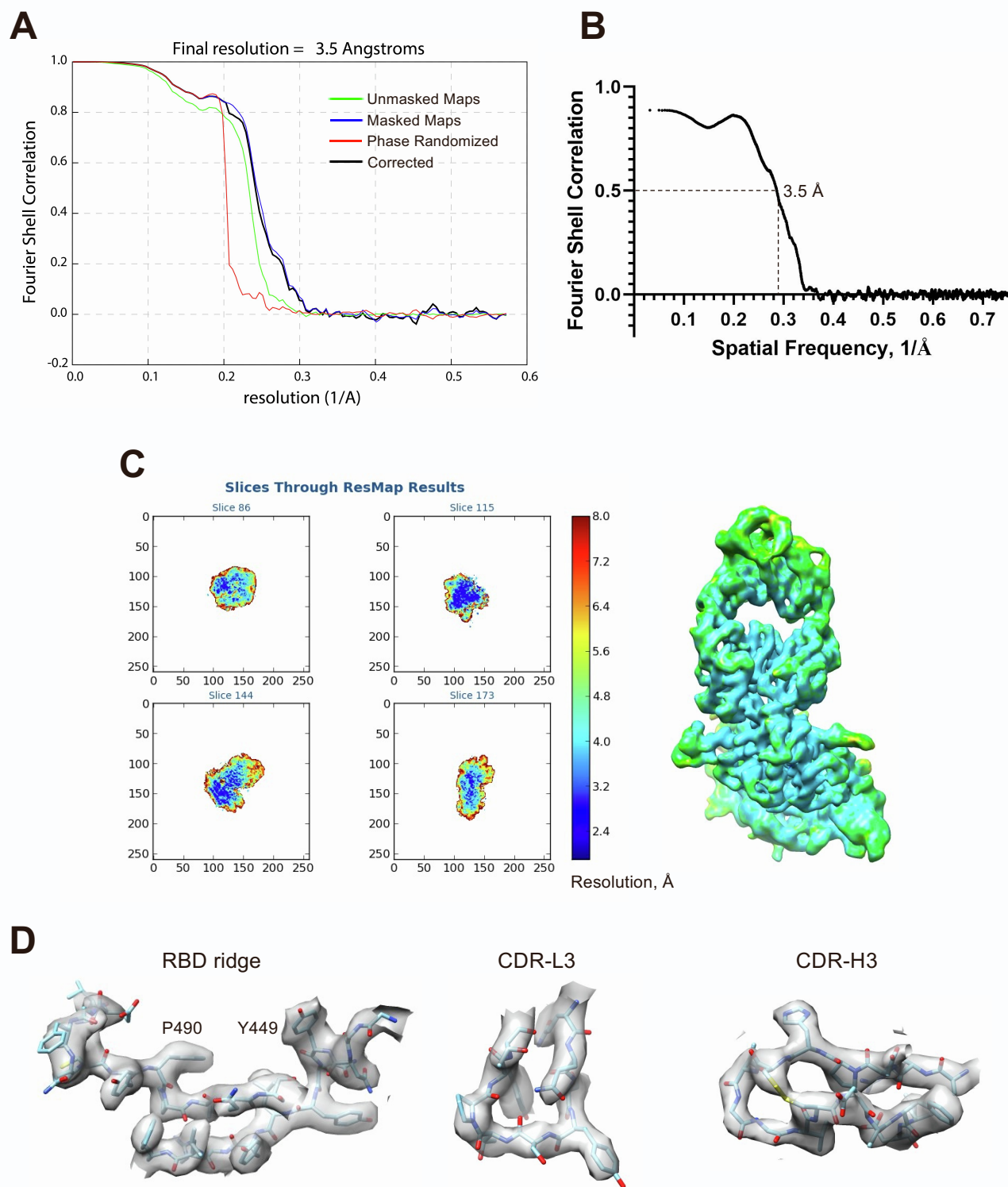


**Figure S11. Validation of the local cryo-EM structure of SARS-CoV-2 receptor binding domain in complex with Fab NA8, related to Figure 4.**

(A) Fourier shell correlation (FSC) plots generated by Relion.

(B) FSC curve between the map and atomic model.

(C) Local resolution determined with ResMap.

(D) Examples of cryo-EM density.

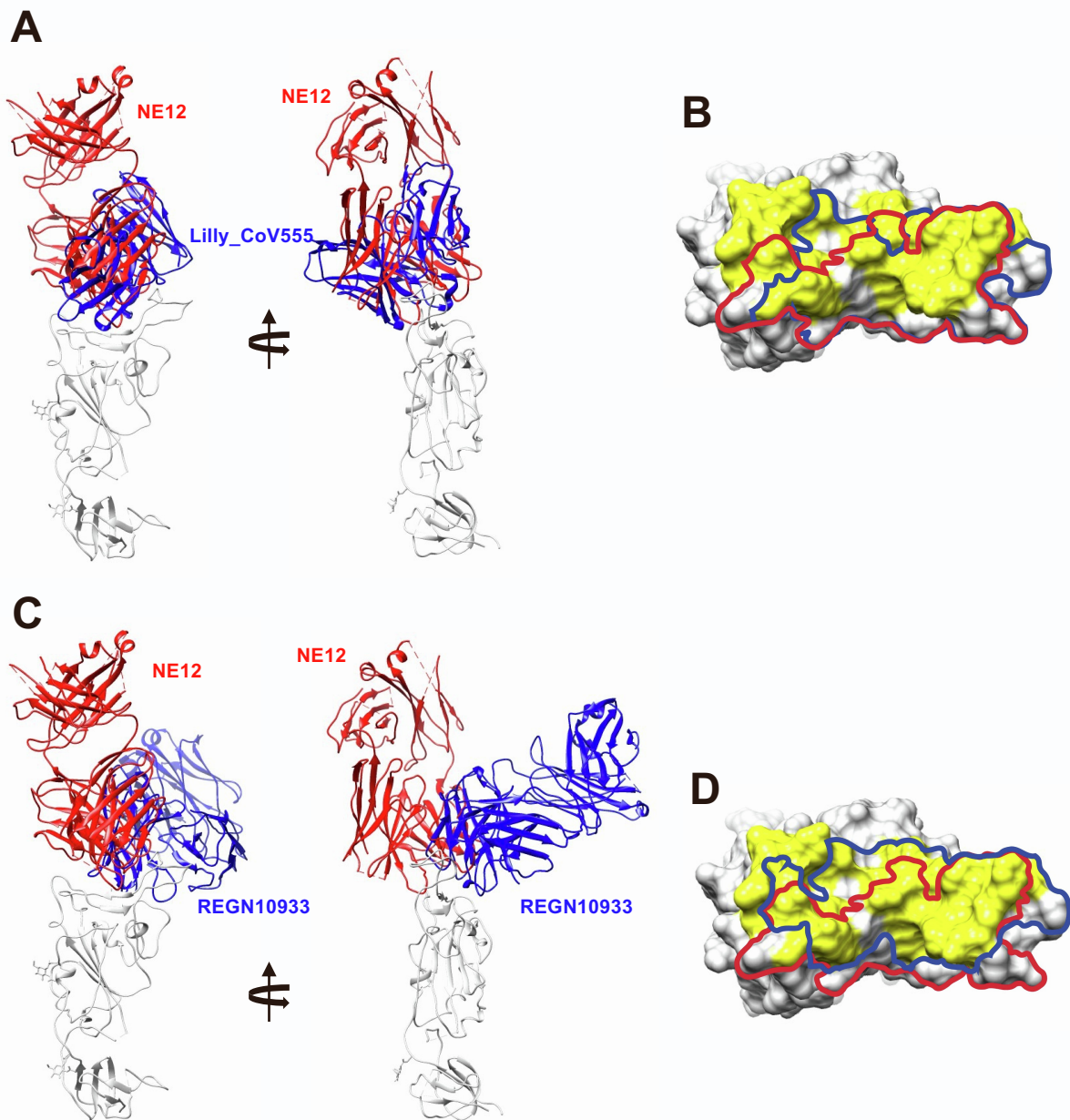


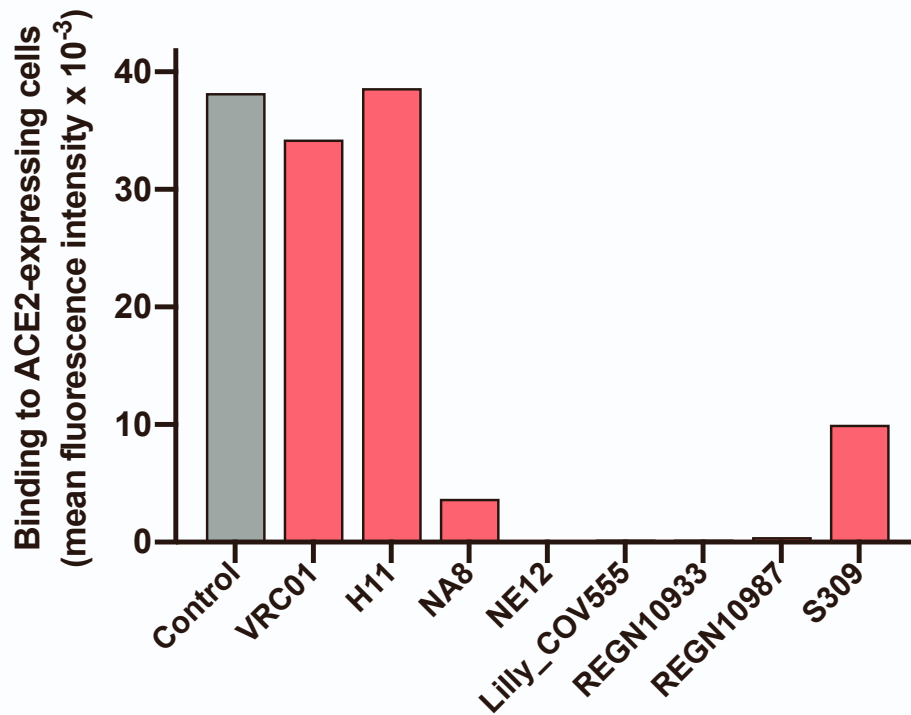
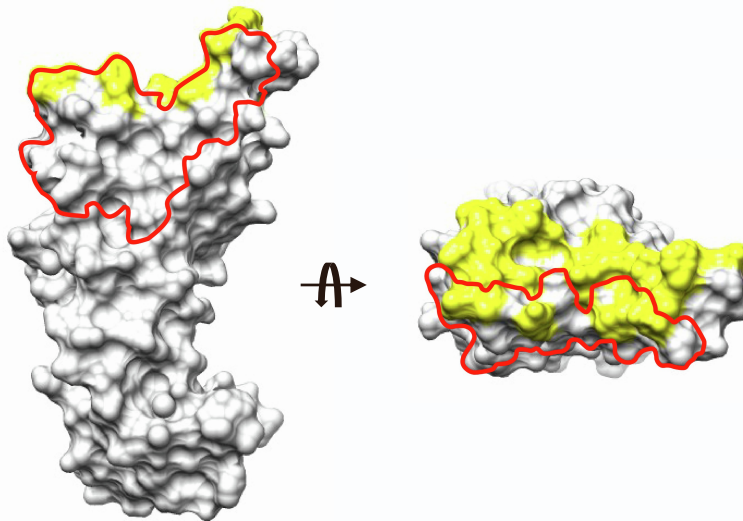
**Figure S12. Comparison of binding modes and epitopes of RBD-directed antibodies NE12, Lilly\_CoV555 and REGN10933, related to Figure 5.**

(A) Cartoon representations of aligned RBD-Fab complexes for NE12 and Lilly\_CoV555 (from PDB 7I3n).

(B) The RBD is shown in surface representation with the epitopes of NE12 and Lilly\_CoV555 outlined with red and blue curves, respectively. Surface areas corresponding to the RBD residues forming the ACE-2 receptor interface are colored yellow.

(C) Cartoon representations of aligned RBD-Fab complexes for NE12 and REGN10933 (from PDB 6xdg).

(D) The RBD is shown in surface representation with the epitopes of NE12 and REGN10933 outlined with red and blue curves, respectively. Surface areas corresponding to the RBD residues forming the ACE-2 receptor interface are colored in yellow.

**A****B**

**Figure S13. Competition of various mAbs with S-6P trimer binding to ACE-2-positive cells, related to Figure 5.**

(A) Ability of monoclonal antibodies against the SARS-CoV-2 spike to block the interaction of the S-6P trimer to ACE2-expressing HEK293 cells. The trimer was directly labeled with phycoerythrin (PE) and pre-incubated with each of the mAbs or with PBS buffer (control) for 30 min before incubation with the cells for 30 min.

(B) Overlap between the NA8 epitope and the ACE2 footprint. The RBD is shown in surface representation. The epitope of NA8 is outlined with a red line. The ACE2 interface is colored in yellow.



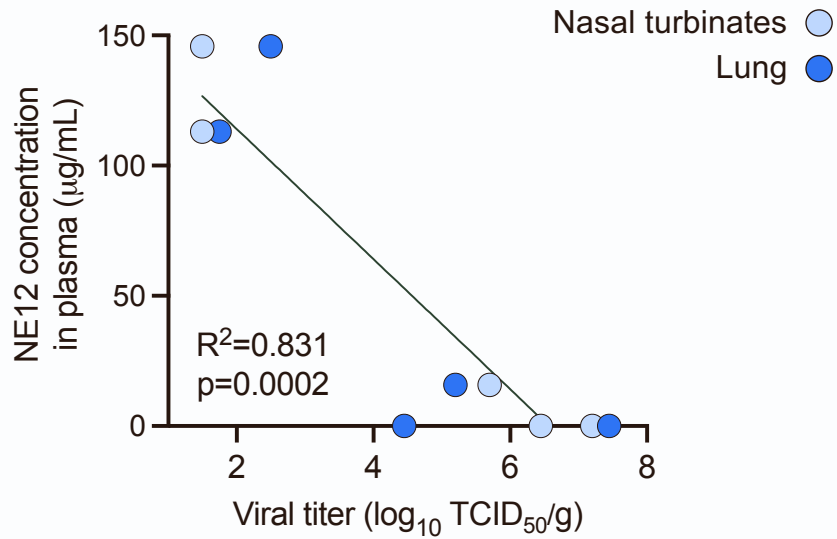


**Figure S14. Plasma concentrations of anti-SARS-CoV-2 spike human antibodies in hamsters treated with mAbs NE12 and NA8, related to Figure 7.** Mean plasma levels of NE12 and NA8 in hamsters treated with the mAbs 24 hours after virus challenge with the original strain, WA-1, or the B.1.351 variant. The mAb concentrations were determined using a specific ELISA with the recombinant S-protein trimer (S-2P) immobilized on the plastic surface. The data represent mean values from 5 animals ( $\pm$  SEM).

**Table S1. Demographic characteristics and neutralizing antibody titers in 12 COVID-19 convalescent plasma donors, related to Figure 1**

<b>Patient number</b>	<b>1</b>	<b>2</b>	<b>3</b>	<b>4</b>	<b>5</b>	<b>6</b>	<b>7</b>	<b>8</b>	<b>9</b>	<b>10</b>	<b>11</b>	<b>12</b>
<b>Age</b>	65	60	53	35	49	40	66	62	58	52	54	61
<b>Gender</b>	F	F	M	M	M	M	F	M	F	F	M	F
<b>Neutralizing antibody titer</b>	80	80	80	80	320	320	320	160	160	640	160	640
<b>Blood collected (mL)</b>	40	35	19	24	24	40	22	28	38	40	32	18

**Table S2. Binding affinity of anti-SARS-CoV-2 Fabs to the S-2P trimer, as measured by surface plasmon resonance, related to Figure 1**

<b>Fab</b>	<b><math>K_D</math> (M)</b>	<b><math>k_d</math> (s<sup>-1</sup>)</b>	<b><math>k_a</math> (1/Ms)</b>
<b>1G8</b>	6.2e-10	2.0e-4	4.6e5
<b>3F6</b>	4.3e-10	8.2e-4	3.9e6
<b>4B6</b>	8.7e-10	1.1e-3	1.3e6
<b>D12</b>	7.2e-10	8.7e-4	1.3e6
<b>NA8</b>	4.6 e-10	1.2e-3	2.8e6
<b>2A12</b>	3.0e-10	8.0e-4	2.7e6
<b>NE8</b>	1.8e-10	5.7e-3	3.1e6
<b>NE12</b>	6.1e-10*	6.5e-4	1.3e6
<b>NG3</b>	2.2e-10	2.0e-4	1.0e6
<b>4B7</b>	1.1e-9	1.7e-3	1.6e6
<b>A7</b>	3.9e-10	7.8e-4	2.2e6
<b>H11</b>	6.5e-9	1.7e-3	2.7e5

\*Constants were determined using BiaEvaluation software. Constants are the average of two different analyses. Only one reliable data set was obtained for 4B7.

**Table S3. Genetic properties of 18 Fabs specific for the spike (S) protein of SARS-CoV-2, related to Figure 1**

Fab	Heavy chain						Light chain				
	VH	JH	DH	HCDR3	CDR3 length	VH SHM	VL	JL	LCDR3	CDR3 length	VL SHM
<b>G6</b>	1-24	5	6-13	CATAPAIAAAAYTGWFDPW	16	4	LV2-14	LJ2	CSSYAGSSVVF	9	9
<b>4A12</b>	3-9	6	2-15	CVRGEILGDDYYRMDVW	15	14	KV1-39	KJ4	CQQSYSTPLTF	9	0
<b>4B7</b>	3-30-3	4	1-26	CARPHSGSYFSHFQDYW	14	8	KV3-20	KJ1	CQQYGSSPWTF	9	0
<b>A7</b>	1-69	6	3-10	CANGAHNWGSGFSYYSYMDVW	20	5	KV3-20	KJ4	CQQYGSSPLTF	9	0
<b>1B1</b>	1-69	6	4-17	CARYIPDFGDYVTPYYYYALDVW	21	15	KV1-39	KJ4	CQQSYSTPLTF	9	0
<b>4C6</b>	3-30	3	4-23	CARSYGGNYLSAFDVW	14	11	KV3-15	KJ3	CQQNNEWPLTF	9	9
<b>H11</b>	1-46	3	3-10	CVYDTGPHAFDIW	11	3	LV1-51	LJ3	CGTWDSLSLVWVF	11	2
<b>1G8</b>	1-2	6	D1-7	CARDRKFDNSWNKYDKGRYGMDVW	21	12	KV1-39	KJ4	CQQSYTLTF	7	6
<b>3F6</b>	1-2	4	3-22	CARVPRNYDRRGLVYEDYFEYW	22	8	KV3-20	KJ2	CQQFGSPPIF	9	6
<b>3B6</b>	3-23	4	3-22	CAKVGRRSNTLIVVATEFDYW	19	14	KV1-39	KJ3	CQQGYSTPPLTF	11	6
<b>4B6</b>	1-69	6	4-11	CARDSTESPLYGMDVW	14	8	KV1-39	KJ2	CQQSYSTPLTF	9	0
<b>D12</b>	3-13	3	3-16	CARGGPLGGGEDAFDMW	15	9	KV1-5	KJ2	CQHYSGYPTYF	9	16
<b>NA8</b>	3-33	3	2-8	CARDPHCTGGVCDAFDLW	16	15	KV1-39	KJ2	CQQSYSTPYTF	9	1
<b>2A12</b>	1-2	4	3-22	CARTLYYYDSSGNLSLDHW	17	7	KV1-39	KJ3	CQQSYSSQWTF	9	24
<b>NE8</b>	1-69	4	2-15	CARGHRYCSGGSCFPYFDYW	18	5	KV1-39	KJ2	CQQSYSTPRTF	9	0
<b>NE12</b>	1-2	6	1-26	CAREETIVGATPPYGLDVW	17	6	KV3-11	KJ5	CQQRSNWPPVTF	10	1
<b>NF8</b>	1-69	4	3-16	CAGVEAYHDSIWGTFAPRYFFGSW	22	14	KV1-39	KJ3	CQQSYSSPPTF	9	0
<b>NG3</b>	1-69	4	5-18	CARVSGYSFGPYFDYW	14	6	KV3-11	KJ3	CQQRSSWPPTF	9	0

**Table S4. Cryo-EM data collection and analysis statistics, related to Figures 3 and 4**

	S-6P in complex with Fab NE12		S-6P in complex with Fab NA8	
<b>Data collection and processing</b>				
Magnification	105,000		105,000	
Voltage (kV)	300		300	
Electron exposure (e <sup>-</sup> /Å <sup>2</sup> )	40		40	
Defocus range (μm)	-1.0 to -2.5		-1.0 to -2.5	
Pixel size (Å)	0.873		0.873	
Symmetry imposed	C1		C1	
Initial particle images (no.)	2,253,882		2,870,476	
Final particle images (no.)	201,607		454,910	
	Consensus map EMDB-26401	Local map EMDB-26402 PDB 7U9O	Consensus map EMDB-26403	Local map EMDB-26404 PDB 7U9P
Map resolution (Å)	3.1	3.4	2.9	3.5
FSC threshold	0.143		0.143	
Map resolution range (Å)	1.9-6.8	3.1-6.8	1.9-8.0	3.1-6.8
<b>Refinement</b>				
Initial model used (PDB code)		6xlu		6xlu
Model resolution (Å)		3.4		3.5
FSC threshold		0.5		0.5
Map sharpening <i>B</i> factor (Å <sup>2</sup> )	-44.4	-125.7	-53.3	-165.1
Model composition				
Non-hydrogen atoms		6563		6126
Protein residues		829		777
Ligands (glycans)		3		4
Water		0		0
<i>B</i> factors (Å <sup>2</sup> ) (mean)				
Protein		58.9		65.8
Ligand		82.1		103.7
Water		N/A		N/A
R.m.s. deviations				
Bond lengths (Å)		0.007		0.013
Bond angles (°)		0.926		1.19
Validation				
MolProbity score		1.44		1.63
Clash score		1.55		2.49
Poor rotamers (%)		0.28		0.15
Ramachandran plot				
Favored (%)		90.34		88.16
Allowed (%)		9.53		11.57
Disallowed (%)		0.13		0.27